Supplementary Information (SI) for Physical Chemistry Chemical Physics.
This journal is © the Owner Societies 2026

Supporting Information for:

Carboxyl-functionalized flavin as efficient heavy-atom-free triplet photosensitizers: A theoretical investigation

Huimin Guo[1,*], Heping Li[1], Chengyu Yang[1]

[1]School of Chemistry, State Key Laboratory of Fine Chemicals, Dalian University of Technology, Dalian, 116024, P. R. China.
*Corresponding author, email: guohm@dlut.edu.cn (H.G.)

This file contains 19 Tables and 19 Figures in 43 pages.

Keywords:
Flavin; Triplet Excited State Lifetime; Photosensitizer; Electron Transfer; Carboxylate

THEORETICAL METHODS

Evaluation of electronic structure at ground state and excited states

DFT and TD-DFT based calculations were performed to investigate electronic structure of methyl flavin carboxylate (McFL, Fig. 1a). Methyl was used to represent the alkyl moieties. The compounds of interest were fully relaxed at B3LYP/6-311G(d) level to get the ground state (S_0) structures.[1-4] Polarizable Continuum Model (PCM) was used to handle the impact of acetyl nitrile (CH_3CN) solvent unless specified.[5-7] The excited structures of FL, McFLs were fully relaxed without any constrain with TD-DFT based calculations at the same level of theory with Gaussian 16.[8] Frequency calculations were performed for all reported structures to insure their nature of minima on the corresponding potential energy surface (PES). The transition dipole moments from T_n to S_0 are evaluated from the quadratic response function[9-11] and the spin−orbit coupling matrix elements are computed at the same level of theory using the effective single-electron approximation in linear response theory with the Dalton program.[12-14] Photophysical properties of these compounds were investigated with Thermal Vibration Correlation Function (TVCF) formalism proposed by Shuai, Peng and coworkers as implemented in MOMAP and integrated with Device Studio.[15-20]

Calculation of photophysical properties of McFLs

The absorption, fluorescence and phosphorescence spectra of compounds, together with the radiative and non-radiative decay rate constants were calculated using MOMAP.[15-19, 21] The absorption and fluorescence spectra were calculated according to eq-S1 and 2:

$$\sigma(\omega)_{abs} = \frac{4\pi^2\omega}{3\hbar c} \times \sum_{v_i,v_f} P_{iv_i}(T) \left|\left\langle \Theta_{f,v_f} \middle| \mu_{fi} \middle| \Theta_{i,v_i} \right\rangle\right|^2 \delta\left(\omega - \omega_{f,v_f,i,v_i}\right) \quad \text{(eq-S1)}$$

$$\sigma(\omega)_{emi} = \frac{4\omega^3}{3\hbar c} \times \sum_{v_i,v_f} P_{iv_i}(T) \left|\left\langle \Theta_{f,v_f} \middle| \mu_{fi} \middle| \Theta_{i,v_i} \right\rangle\right|^2 \delta\left(\omega_{i,v_i,f,v_f} - \omega\right) \quad \text{(eq-S2)}$$

where $P_{iv_i}(T)$ is the Boltzmann population of the vibrational manifolds in the initial state, $\mu_{fi} = \langle \Phi_f | \mu | \Phi_i \rangle$ is the electronic transition dipole moment between the initial state i and final state f calculated according to the Frank-Condon approximation, v_i/v_f is vibrational quantum number of state i/f, Θ_{f,v_f} is the v_fth vibrational state of final state f, ω is the radiation frequency and $\omega_{i,v_i,f,v_f} = \omega_{f,v_f} - \omega_{i,v_i}$, respectively. The absorption and emission rate constants were calculated as the integration of the spectra.[21-24]

For the non-radiative decay, applying the second-order perturbation approximation, the rate constants were calculated as:

$$k_{f\leftarrow i} = \frac{2\pi}{\hbar}\sum_{v_i,v_f} P_{iv_i}\left|H'_{fv_f,iv_i} + \sum_{n,v_n}\frac{H'_{fv_f,nv_n}H'_{nv_n,iv_i}}{E_{iv_i}-E_{nv_n}}\right|^2 \times \delta\left(E_{iv_i} - E_{fv_f}\right) \quad \text{(eq-S3)}$$

where, v_i/v_f is vibrational quantum number of state i/f and H' is the interaction between 2 different Born-Oppenheimer states and calculated as $H'\psi_{iv_i} = H^{NA}\Phi_i(r:Q)\Theta_{iv_i}(Q) + H^{SO}\Phi_i(r:Q)\Theta_{iv_i}(Q)$, where H^{NA} is the non-adiabatic coupling operator, H^{SO} is the spin-orbital coupling operator, r and Q are the electronic and nuclear normal mode coordinates.[25]

By applying a displayed oscillator mode and short time approximation, the internal conversion rate constant can be derived as:

$$logk_{ic,l}(\omega_{if}) \propto -\left(-\omega_{if} + \omega_i + \sum_{j(j\neq l)} S_j\omega_j\right)^2/2\sum_{j(j\neq l)} S_j{\omega_j}^2(2n_j+1) \quad \text{(eq-S3')}$$

where $S_j = \omega_j {D_j}^2/2\hbar$ is the Huang-Rhys factor and D_j is the displacement of *j*th mode, n_j is the phonon distribution function and $\lambda_j = S_j\hbar\omega_j$ is the reorganization of *j*th accepting mode.

By applying short-time approximation under the framework of the displaced harmonic oscillator model, the non-radiative decay rate constant for $T_1 \rightarrow S_0$ can be calculated as:

$$k'_{ISC} = exp\left[-\frac{(\Delta E_{ad}-\sum_k\lambda_k)^2}{4\sum_k\lambda_k E_k} + ln\left(\frac{1}{\hbar}|\langle S_0|H^{SO}|T_1\rangle|^2\sqrt{\frac{\pi}{\sum_k\lambda_k E_k}}\right)\right] \quad \text{(eq-S3'')}$$

where ΔE_{ad} is the adiabatic excitation energy; $\lambda_k = S_k\hbar\omega_k = {\omega_k}^2{D_k}^2/2$ is the reorganization energy for the *k*th mode; S_k and D_k are the Huang-Rhys factor and displacement of the mode with frequency of ω_k, respectively; E_k is the average vibration energy.

The transition dipole moment for phosphorescence was calculated as eq-S4:

$$\mu_{ST_\kappa} = \sum_k^{\{singlets\}}\frac{\langle S|\mu|\,{}^1k\rangle\langle\,{}^1k|H^{SO}|T_\kappa\rangle}{{}^3E_T^0 - {}^1E_k^0} + \sum_n^{\{triplets\}}\sum_{\kappa'=1}^{3}\frac{\langle S|H^{SO}|\,{}^3n_{\kappa'}\rangle\langle\,{}^3n_{\kappa'}|\mu|T_\kappa\rangle}{{}^1E_S^0 - {}^3E_n^0} \quad \text{(eq-S4)}$$

where κ is the magnetic quantum number, n and k are the intermediate triplet and singlet electronic states, respectively. Applying the Franck-Condon approximation, the phosphorescence spectra were calculated as eq-S5[19]:

$$\sigma_{ph}(\omega,T) = \frac{4\omega^3}{3\hbar c^3}\times\sum_{v_i,v_f} P_{iv_i}(T)\left|\left\langle\Theta_{f,v_f}\middle|\mu_{ST}\middle|\Theta_{i,v_i}\right\rangle\right|^2\delta\left(\omega_{i,v_i,f,v_f} - \omega\right) \quad \text{(eq-S5)}$$

The radiative decay rate constant was calculated as the integration of the phosphorescence spectra.

The intersystem crossing rate constant can be calculated as:

$$k_{ISC} = k_{ISC}^{(0)} + k_{ISC}^{(1)} + k_{ISC}^{(2)} \quad \text{(eq-S6)}$$

where:

$$k_{ISC}^{(0)} = \frac{2\pi}{\hbar}\sum_{v_i,v_f} P_{iv_i}\left|H'_{fv_f,iv_i}\right|^2 \times \delta\left(E_{iv_i} - E_{fv_f}\right) \quad \text{(eq-S7)}$$

$$k_{ISC}^{(1)} = \frac{2\pi}{\hbar}\sum_{v_i,v_f} P_{iv_i} 2Re(H'_{fv_f,iv_i}\sum_{n,v_n}\frac{H'_{fv_f,nv_n}H'_{nv_n,iv_i}}{E_{iv_i}-E_{nv_n}}) \times \delta\left(E_{iv_i} - E_{fv_f}\right) \quad \text{(eq-S8)}$$

$$k_{ISC}^{(2)} = \frac{2\pi}{\hbar}\sum_{v_i,v_f} P_{iv_i}\left|\sum_{n,v_n}\frac{H'_{fv_f,nv_n}H'_{nv_n,iv_i}}{E_{iv_i}-E_{nv_n}}\right|^2 \times \delta\left(E_{iv_i} - E_{fv_f}\right) \quad \text{(eq-S9)}$$

where H' is the interaction between 2 different Born-Oppenheimer states and calculated as $H'\psi_{iv_i} = H^{NA}\Phi_i(r;Q)\Theta_{iv_i}(Q) + H^{SO}\Phi_i(r;Q)\Theta_{iv_i}(Q)$, where H^{NA} is the non-adiabatic coupling operator, H^{SO} is the spin-orbital coupling operator. The intersystem crossing rate constant can be calculated using the above methods by switching the initial and final states. More details on calculation of these spectra and rate constants can be found in Ref. 15-24.

The triplet quantum yield (Φ_T) of these McFLs were calculated as:

$$\Phi_T = \sum k_{ISC,\,S_1\to T_n} / \left(k_{f,\,S_1\to S_0} + k_{IC,S_1\to S_0} + \sum k_{ISC,S_1\to T_n}\right) \quad \text{(eq-S10)}$$

In eq-S1, $k_{f,\,S_1\to S_0}$, $k_{IC,S_1\to S_0}$, and $\sum k_{ISC,S_1\to T_n}$ are the rate constants for FE, IC, and the sum of ISC from S_1 to energy allowed triplet excited states, respectively.

The Kinetic Model

Based on the calculated photophysical properties and rate constants, the photophysical processes involved for evolution of FL and McFLs under continuous irradiation can be derived. They start with the population of FL and McFLs to spin allowed S_1. Then, the excited FL and McFLs would evolve via IC and FE from S_1. In absence of ICT for FL and McFLs, energy downhill ISC $S_1 \rightarrow T_n$ processes may also take place competing with IC and FE. After reaching T_n, excited FL and McFLs would decay into spin allowed T_1 very fast. Finally, these excited FL and McFLs at T_1 would decay via PE or nonradiative decay back to S_0.

The equations describing concentration of McFLs at S_0, S_1, T_1, T_2 and T_3 as functions of time can be written as the following:

$$\frac{dc_{S_0}}{dt} = -k_{ad}c_{S_0} + c_{S_1}\left(k_f + k_{IC}\right) + \sum_1^3 c_{T_n}\left[k_{p(T_n-S_0)} + k_{ISC(T_n-S_0)}\right] \quad \text{(eq-S11)}$$

$$\frac{dc_{S_1}}{dt} = k_{ad}c_{S_0} - c_{S_1}\left(k_f + k_{IC} + \sum_1^3 c_{T_n}\, k_{ISC(S_1-T_n)}\right) + \sum_1^3 c_{T_n}\, k_{RISC(T_n-S_1)} \quad \text{(eq-S12)}$$

$$\frac{dc_{T_1}}{dt} = k_{ISC(S_1-T_1)}c_{S_1} - c_{T_1}\left(k_{p(T_1-S_0)} + k_{ISC(T_1-S_0)} + k_{RISC(T_1-S_1)}\right) + k_{IC(T_3-T_1)}c_{T_3} + k_{IC(T_2-T_1)}c_{T_2} \quad \text{(eq-S13)}$$

$$\frac{dc_{T_2}}{dt} = k_{ISC(S_1-T_2)}c_{S_1} + k_{IC(T_3-T_2)}c_{T_3} - c_{T_2}\left(k_{p(T_2-S_0)} + k_{ISC(T_2-S_0)} + k_{IC(T_2-T_1)} + k_{RISC(T_2-S_1)}\right) \quad \text{(eq-S14)}$$

$$\frac{dc_{T_3}}{dt} = k_{ISC(S_1-T_3)}c_{S_1} - c_{T_3}\left(k_{p(T_3-S_0)} + k_{ISC(T_3-S_0)} + k_{IC(T_3-T_1)} + k_{IC(T_3-T_2)} + k_{RISC(T_3-S_1)}\right) \quad \text{(eq-S15)}$$

Furthermore,

$$k_{ad} = \sigma \mathrm{F} \quad \text{(eq-S16)}$$

$$\mathrm{F} = \frac{\mathrm{P}}{\mathrm{Ahv}} = 6.79 \times 10^{19}\,\mathrm{Photons \cdot cm^{-2} \cdot s^{-1}} \quad \text{(eq-S17)}$$

$$10^{-\varepsilon \mathrm{cd}} = \mathrm{e}^{-\sigma \mathrm{nd}} \quad \text{(eq-S18)}$$

$$\sigma = \varepsilon \ln 10 \frac{\mathrm{c}}{\mathrm{n}} = \varepsilon\alpha = \alpha\varepsilon \quad \text{(eq-S19)}$$

$$\alpha = 3.82 \times 10^{-21}\,\mathrm{mol \cdot cm^3 \cdot L^{-1}} \quad \text{(eq-S20)}$$

where σ is the absorption cross-section of sensitizer, P is the input power of light radiation at 455 nm, that is 30 W, ε is the molecular extinction constant ($dm^3mol^{-1}cm^{-1}$), c is the concentration, in mol L^{-1}, n is the particle density, in cm^{-3}, d is path depth, in cm, α is the conversion constant, v is the frequency, A is the cross-section of light, that is 1 cm^2.

By solving equations eq-S11 to eq-S15 iteratively, with eq-S16 to eq-S20, calculated photophysical properties in Tables 1, 2 and 3, and assuming McFLs are dissolved in acetyl nitrile solution of 0.033 mol/L at 298 K under continuous irradiation at wavelength of 455 nm, the steady state concentration of McFLs at S_0, S_1, T_1, T_2 and T_3 can be obtained (Table 5).

Table S1a. Electronic transitions involved in the excitation of FL.

	Energy	f	Composition	Percentage [a]	Character
$S_0 \rightarrow S_1$	3.02 eV/410 nm	0.2013	59→60	96.54%	π→π*
$S_0 \rightarrow S_2$	3.35 eV/370 nm	0.0008	56→60	54.94%	n→π*
			57→60	42.74%	n→π*
$S_0 \rightarrow S_3$	3.50 eV/354 nm	0.0000	57→60	52.69%	n→π*
			56→60	42.47%	n→π*
$S_0 \rightarrow S_4$	3.75 eV/331 nm	0.1821	58→60	92.42%	π→π*
$S_0 \rightarrow S_5$	4.18 eV/297 nm	0.0000	54→60	92.61%	n→π*
$S_0 \rightarrow S_6$	4.24 eV/292 nm	0.0111	55→60	92.35%	π→π*
$S_0 \rightarrow S_7$	4.69 eV/265 nm	0.0004	52→60	93.57%	n→π*
$S_0 \rightarrow S_8$	4.82 eV/257 nm	0.0158	53→60	85.50%	π→π*
			58→61	11.10%	π→π*
$S_0 \rightarrow S_9$	4.90 eV/259 nm	0.7373	59→61	87.04%	π→π*
$S_0 \rightarrow S_{10}$	5.23 eV/237 nm	0.0503	56→61	62.55%	n→π*
			57→61	30.47%	n→π*
$S_0 \rightarrow T_1$	2.15 eV/576 nm	0.0000	59→60	96.79%	π→π*
$S_0 \rightarrow T_2$	2.73 eV/454 nm	0.0000	58→60	86.92%	π→π*
$S_0 \rightarrow T_3$	2.90 eV/428 nm	0.0000	56→60	69.71%	n→π*
			57→60	18.76%	n→π*
			52→60	8.25%	n→π*
$S_0 \rightarrow T_4$	3.28 eV/378 nm	0.0000	57→60	71.39%	n→π*
			56→60	17.20%	n→π*
$S_0 \rightarrow T_5$	3.61 eV/343 nm	0.0000	55→60	67.59%	π→π*
			59→61	21.90%	π→π*

[a] Orbital transition contribution during excitation.

Table S1b. Electronic transitions involved in the excitation of FL with inclusion of DFT-D3.

	Energy	f	Composition	Percentage [a]	Character
$S_0 \rightarrow S_1$	2.93 eV/423 nm	0.3372	59→60	98.68%	π→π*
$S_0 \rightarrow S_2$	3.34 eV/371 nm	0.0012	56→60	55.93%	n→π*
			57→60	41.64%	n→π*
$S_0 \rightarrow S_3$	3.49 eV/355 nm	0.0000	57→60	53.71%	n→π*
			56→60	41.38%	n→π*
$S_0 \rightarrow S_4$	3.68 eV/337 nm	0.2864	58→60	96.66%	π→π*
$S_0 \rightarrow S_5$	4.18 eV/297 nm	0.0000	54→60	92.56%	n→π*
$S_0 \rightarrow S_6$	4.22 eV/294 nm	0.0189	55→60	93.83%	π→π*
$S_0 \rightarrow S_7$	4.68 eV/265 nm	0.0006	52→60	93.59%	n→π*
$S_0 \rightarrow S_8$	4.74 eV/261 nm	0.9716	59→61	88.59%	π→π*
			53→60	4.46%	π→π*
$S_0 \rightarrow S_9$	4.81 eV/258 nm	0.0154	53→60	84.27%	π→π*
			58→61	8.68%	π→π*
$S_0 \rightarrow S_{10}$	5.22 eV/238 nm	0.0568	59→62	58.28%	n→π*
			58→61	35.01%	n→π*
$S_0 \rightarrow T_1$	2.15 eV/576 nm	0.0000	59→60	96.84%	π→π*
$S_0 \rightarrow T_2$	2.74 eV/453 nm	0.0000	58→60	87.03%	π→π*
$S_0 \rightarrow T_3$	2.90 eV/428 nm	0.0000	56→60	70.28%	n→π*
			57→60	18.14%	n→π*
			52→60	8.31%	n→π*
$S_0 \rightarrow T_4$	3.28 eV/378 nm	0.0000	57→60	71.96%	n→π*
			56→60	16.59%	n→π*
$S_0 \rightarrow T_5$	3.61 eV/343 nm	0.0000	55→60	68.98%	π→π*
			59→61	20.74%	π→π*

[a] Orbital transition contribution during excitation.

Table S2a. Electronic transitions involved in the excitation of 7McFL.

	Energy	f	Composition	Percentage [a]	Character
$S_0 \rightarrow S_1$	3.06 eV/405 nm	0.2426	74→75	96.70%	π→π*
$S_0 \rightarrow S_2$	3.33 eV/372 nm	0.0008	71→75	52.54%	n→π*
			72→75	36.81%	π→π*
$S_0 \rightarrow S_3$	3.47 eV/358 nm	0.0001	72→75	43.09%	π→π*
			71→75	30.82%	n→π*
			68→75	14.22%	n→π*
$S_0 \rightarrow S_4$	3.79 eV/327 nm	0.0889	73→75	83.17%	π→π*
			74→76	13.64%	π→π*
$S_0 \rightarrow S_5$	4.14 eV/300 nm	0.0000	74→76	59.52%	π→π*
			70→75	13.82%	π→π*
			73→75	10.11%	π→π*
$S_0 \rightarrow S_6$	4.19 eV/296 nm	0.0297	68→75	46.68%	n→π*
			65→75	13.03%	n→π*
$S_0 \rightarrow S_7$	4.24 eV/293 nm	0.0000	70→75	56.81%	π→π*
			74→76	20.12%	π→π*
$S_0 \rightarrow S_8$	4.48 eV/277 nm	0.9509	65→75	49.48%	n→π*
			68→75	13.85%	n→π*
$S_0 \rightarrow S_9$	4.69 eV/264 nm	0.0004	73→76	47.58%	π→π*
			70→75	21.93%	π→π*
			67→75	11.27%	π→π*
$S_0 \rightarrow S_{10}$	4.71 eV/264 nm	0.0312	69→76	57.26%	n→π*
			69→75	12.94%	n→π*
$S_0 \rightarrow T_1$	2.20 eV/563 nm	0.0000	74→75	95.66%	π→π*
$S_0 \rightarrow T_2$	2.78 eV/445 nm	0.0000	72→75	80.32%	π→π*
			74→76	6.88%	π→π*
$S_0 \rightarrow T_3$	2.88 eV/430 nm	0.0000	71→75	69.30%	n→π*
			73→75	19.10%	n→π*
			65→75	7.87%	n→π*
$S_0 \rightarrow T_4$	3.24 eV/382 nm	0.0000	73→76	70.94%	π→π*
			71→75	17.65%	π→π*
$S_0 \rightarrow T_5$	3.44 eV/360 nm	0.0000	74→75	77.42%	π→π*
			72→75	9.80%	π→π*

[a] Orbital transition contribution during excitation.

Table S2b. Electronic transitions involved in the excitation of 7McFL calculated with DFT-D3.

	Energy	f	Composition	Percentage [a]	Character
$S_0 \rightarrow S_1$	2.97 eV/417 nm	0.3992	74→75	98.59%	π→π*
$S_0 \rightarrow S_2$	3.32 eV/373 nm	0.0012	71→75	50.12%	n→π*
			72→75	47.04%	π→π*
$S_0 \rightarrow S_3$	3.45 eV/358 nm	0.0001	73→75	48.49%	π→π*
			71→75	46.79%	n→π*
			68→75	2.59%	n→π*
$S_0 \rightarrow S_4$	3.75 eV/331 nm	0.1779	72→75	92.94%	π→π*
			74→76	5.45%	π→π*
$S_0 \rightarrow S_5$	4.13 eV/300 nm	0.0000	68→75	79.00%	π→π*
			69→75	13.81%	π→π*
			73→75	2.52%	π→π*
$S_0 \rightarrow S_6$	4.16 eV/298 nm	0.0719	70→75	78.72%	n→π*
			74→76	16.52%	n→π*
$S_0 \rightarrow S_7$	4.23 eV/293 nm	0.0000	69→75	82.91%	π→π*
			68→75	13.54%	π→π*
$S_0 \rightarrow S_8$	4.33 eV/286 nm	1.1521	74→76	76.29%	n→π*
			70→75	18.25%	n→π*
$S_0 \rightarrow S_9$	4.69 eV/265 nm	0.0006	73→76	82.77%	π→π*
			70→75	10.79%	π→π*
$S_0 \rightarrow S_{10}$	4.70 eV/264 nm	0.0225	69→76	48.89%	n→π*
			69→75	40.55%	n→π*
$S_0 \rightarrow T_1$	2.20 eV/563 nm	0.0000	74→75	95.74%	π→π*
$S_0 \rightarrow T_2$	2.78 eV/445 nm	0.0000	72→75	81.08%	π→π*
			74→76	6.83%	π→π*
$S_0 \rightarrow T_3$	2.88 eV/430 nm	0.0000	71→75	70.33%	n→π*
			73→75	18.15%	n→π*
			65→75	7.96%	n→π*
$S_0 \rightarrow T_4$	3.24 eV/383 nm	0.0000	73→75	72.45%	π→π*
			71→75	16.58%	π→π*
$S_0 \rightarrow T_5$	3.45 eV/360 nm	0.0000	74→76	77.15%	π→π*
			72→75	9.77%	π→π*

[a] Orbital transition contribution during excitation.

Table S3. Electronic transitions involved in the excitation of 8McFL.

	Energy	f	Composition	Percentage	Character
$S_0 \rightarrow S_1$	2.90 eV/427 nm	0.2186	74→75	97.41%	π→π*
$S_0 \rightarrow S_2$	3.23 eV/384 nm	0.0007	71→75	50.08%	n→π*
			72→75	37.18%	π→π*
$S_0 \rightarrow S_3$	3.37 eV/368 nm	0.0000	72→75	40.33%	π→π*
			71→75	30.83%	n→π*
			68→75	14.75%	n→π*
$S_0 \rightarrow S_4$	3.70 eV/335 nm	0.2441	73→75	93.66%	π→π*
$S_0 \rightarrow S_5$	4.02 eV/308 nm	0.0000	74→76	40.08%	π→π*
			70→75	38.17%	π→π*
			67→75	11.36%	π→π*
$S_0 \rightarrow S_6$	4.06 eV/305 nm	0.0001	69→75	52.66%	n→π*
			69→76	13.01%	n→π*
$S_0 \rightarrow S_7$	4.10 eV/303 nm	0.0113	68→75	43.35%	π→π*
$S_0 \rightarrow S_8$	4.58 eV/271 nm	0.0003	65→75	54.38%	n→π*
			68→75	12.12%	n→π*
$S_0 \rightarrow S_9$	4.63 eV/268 nm	0.4617	70→75	53.92%	π→π*
			74→76	35.97%	π→π*
$S_0 \rightarrow S_{10}$	4.69 eV/264 nm	0.1020	67→75	35.28%	n→π*
			74→77	25.72%	n→π*
			73→76	16.66%	n→π*
			74→76	12.20%	n→π*
$S_0 \rightarrow T_1$	2.07 eV/599 nm	0.0000	74→75	96.83%	π→π*
$S_0 \rightarrow T_2$	2.66 eV/466 nm	0.0000	72→75	84.43%	π→π*
$S_0 \rightarrow T_3$	2.82 eV/439 nm	0.0000	71→75	67.65%	n→π*
			73→75	19.44%	n→π*
$S_0 \rightarrow T_4$	3.16 eV/392 nm	0.0000	73→76	66.52%	n→π*
			71→75	18.82%	n →π*
$S_0 \rightarrow T_5$	3.48 eV/356 nm	0.0000	70→75	55.58%	n→π*
			74→75	30.47%	n→π*

Table S4. Electronic transitions involved in the excitation of DcFL.

	Energy	f	Composition	Percentage	Character
$S_0 \rightarrow S_1$	2.93 eV/423 nm	0.1825	76→77	97.62%	π→π*
$S_0 \rightarrow S_2$	3.16 eV/393 nm	0.0006	75→77	60.69%	n→π*
			74→77	34.89%	n→π*
$S_0 \rightarrow S_3$	3.29 eV/377 nm	0.0001	74→77	60.77%	n→π*
			75→77	33.17%	n→π*
$S_0 \rightarrow S_4$	3.67 eV/338 nm	0.0397	76→78	64.37%	π→π*
			73→77	32.29%	π→π*
$S_0 \rightarrow S_5$	3.94 eV/315 nm	0.0000	71→77	65.16%	n→π*
			70→77	25.43%	n→π*
$S_0 \rightarrow S_6$	3.99 eV/312 nm	0.0196	72→77	89.42%	π→π*
$S_0 \rightarrow S_7$	4.01 eV/309 nm	0.0001	70→77	58.59%	n→π*
			71→77	20.10%	n→π*
			71→78	10.73%	n→π*
$S_0 \rightarrow S_8$	4.11 eV/302 nm	0.8628	73→77	54.65%	π→π*
			76→78	32.66%	π→π*
$S_0 \rightarrow S_9$	4.31 eV/288 nm	0.0002	75→78	53.57%	n→π*
			74→78	40.05%	n→π*
$S_0 \rightarrow S_{10}$	4.40 eV/282 nm	0.0000	74→78	54.18%	n→π*
			75→78	36.66%	n→π*
$S_0 \rightarrow T_1$	2.11 eV/587 nm	0.0000	76→77	95.41%	π→π*
$S_0 \rightarrow T_2$	2.78 eV/446 nm	0.0000	74→77	63.03%	n→π*
			75→77	22.99%	n→π*
$S_0 \rightarrow T_3$	2.79 eV/445 nm	0.0000	73→77	70.57%	π→π*
			76→78	14.03%	π→π*
$S_0 \rightarrow T_4$	3.05 eV/405 nm	0.0000	76→78	75.39%	π→π*
			73→77	17.77%	π→π*
$S_0 \rightarrow T_5$	3.06 eV/405 nm	0.0000	75→77	65.06%	n→π*
			74→77	20.88%	n→π*

Table S5. Electronic transitions involved in the excitation of DBFL.

	Energy	f	Composition	Percentage	Character
$S_0 \rightarrow S_1$	2.91 eV/427 nm	0.2562	93→94	96.90%	π→π*
$S_0 \rightarrow S_2$	3.29 eV/377 nm	0.0007	91→94	55.06%	n→π*
			90→94	42.28%	n→π*
$S_0 \rightarrow S_3$	3.41 eV/363 nm	0.0001	90→94	55.24%	n→π*
			91→94	40.41%	n→π*
$S_0 \rightarrow S_4$	3.61 eV/343 nm	0.2527	92→94	93.67%	n→π*
			93→95	3.23%	π→π*
$S_0 \rightarrow S_5$	4.07 eV/304 nm	0.0000	86→94	79.08%	n→π*
			88→94	14.59%	n→π*
$S_0 \rightarrow S_6$	4.09 eV/302 nm	0.0057	87→94	55.99%	π→π*
			89→94	41.67%	π→π*
$S_0 \rightarrow S_7$	4.14 eV/299 nm	0.0000	88→94	84.66%	n→π*
			86→94	13.97%	n→π*
$S_0 \rightarrow S_8$	4.17 eV/297 nm	0.0153	89→94	52.71%	π→π*
			87→94	37.92%	π→π*
$S_0 \rightarrow S_9$	4.59 eV/270 nm	0.0000	93→96	95.72%	π→n*
			89→96	3.57%	π→n*
$S_0 \rightarrow S_{10}$	4.66 eV/266 nm	0.0004	83→94	86.12%	n→π*
			85→94	7.18%	n→π*
$S_0 \rightarrow T_1$	2.09 eV/594 nm	0.0000	93→94	95.51%	π→π*
$S_0 \rightarrow T_2$	2.68 eV/463 nm	0.0000	92→94	82.80%	n→π*
			93→95	4.59%	π→π*
$S_0 \rightarrow T_3$	2.88 eV/431 nm	0.0000	90→94	70.37%	n→π*
			91→94	18.52%	n→π*
$S_0 \rightarrow T_4$	3.19 eV/389 nm	0.0000	91→94	71.87%	n→π*
			90→94	16.89%	n→π*
$S_0 \rightarrow T_5$	3.49 eV/355 nm	0.0000	93→95	35.74%	π→π*
			87→94	33.46%	π→π*
			89→94	21.15%	π→π*

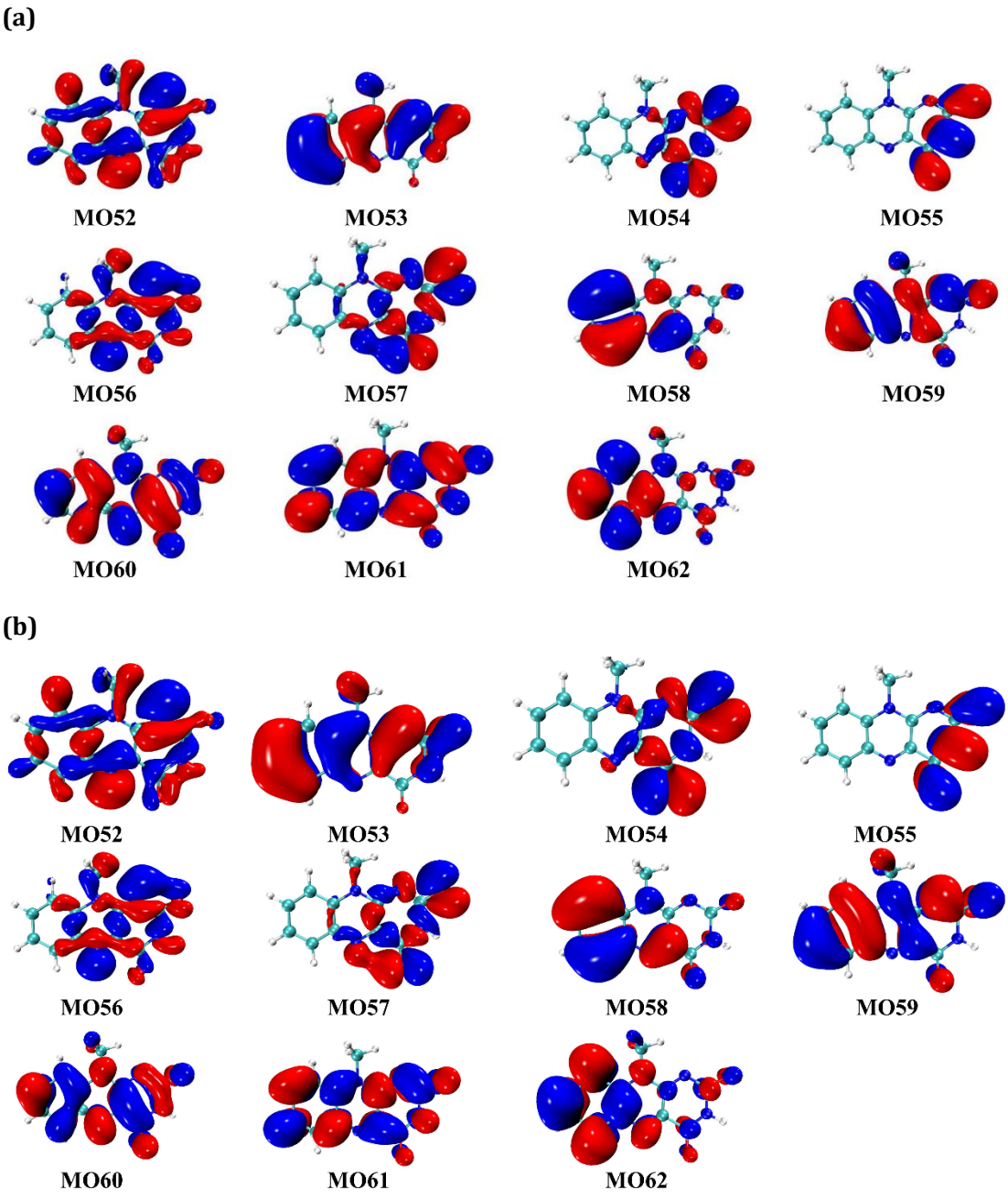

Fig. S1 Isosurface plots of frontier molecular orbitals of FL involved in electronic transitions contribute to UV-vis absorption calculated without(a) and with DFT-D3(b). (Isovalue: ±0.02 a.u.; C: Cyan; O: Red; N: Blue; H: White.)

(a)

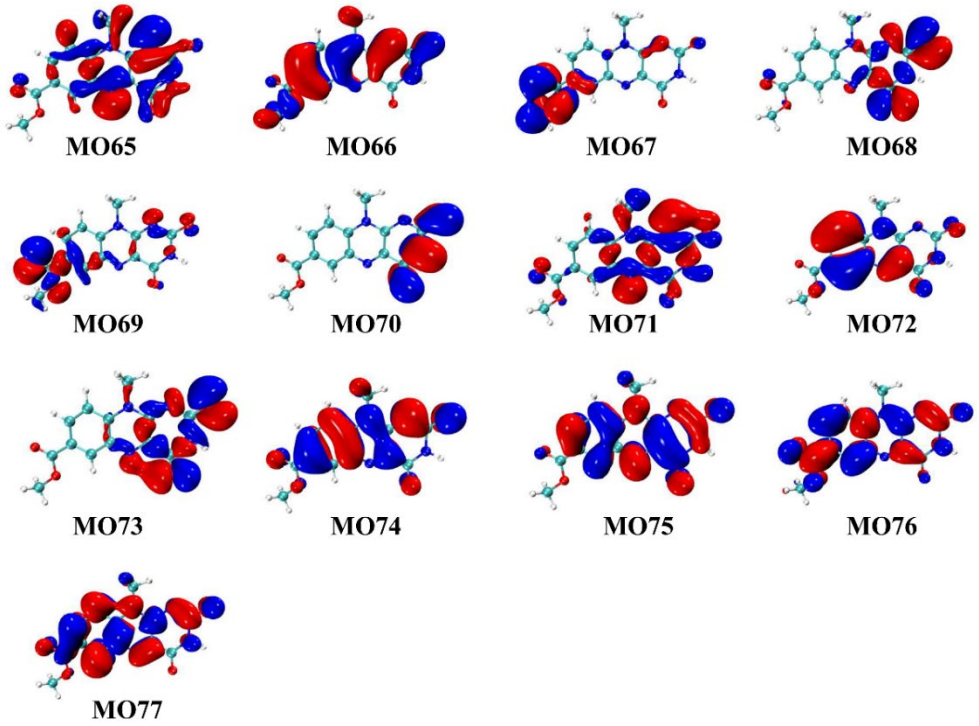

(b)

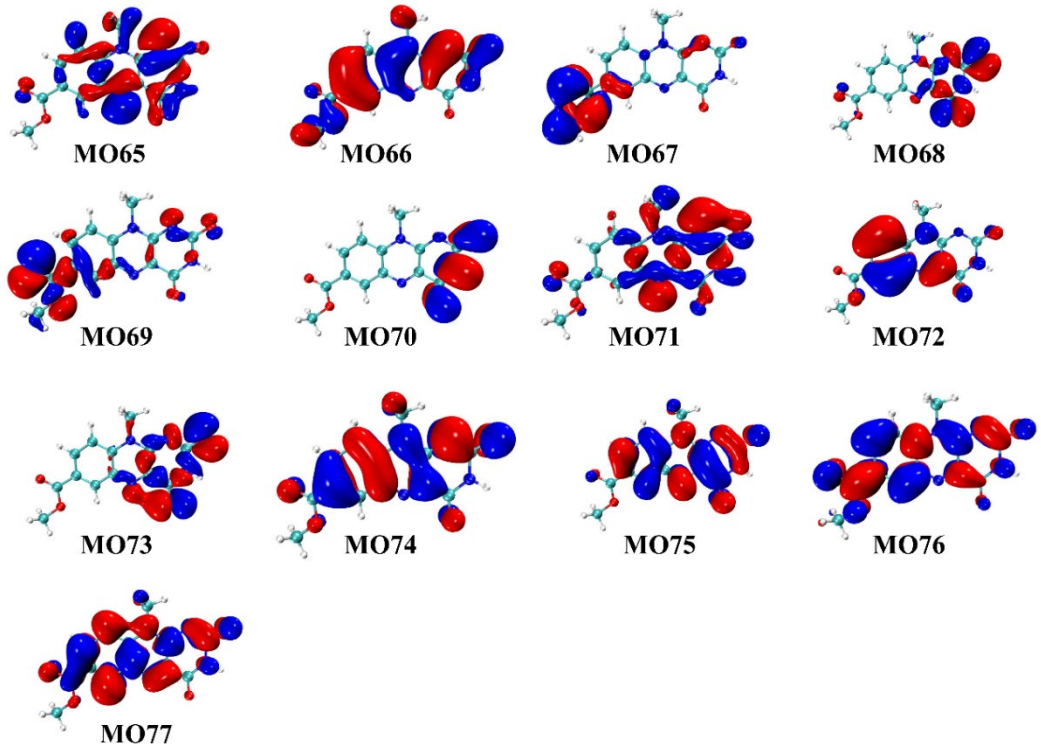

Fig. S2 Isosurface plots of frontier molecular orbitals of 7McFL involved in electronic transitions contribute to UV-vis absorption calculated without (a) and with DFT-D3(b). (Isovalue: ±0.02 a.u.; C: Cyan; O: Red; N: Blue; H: White.)

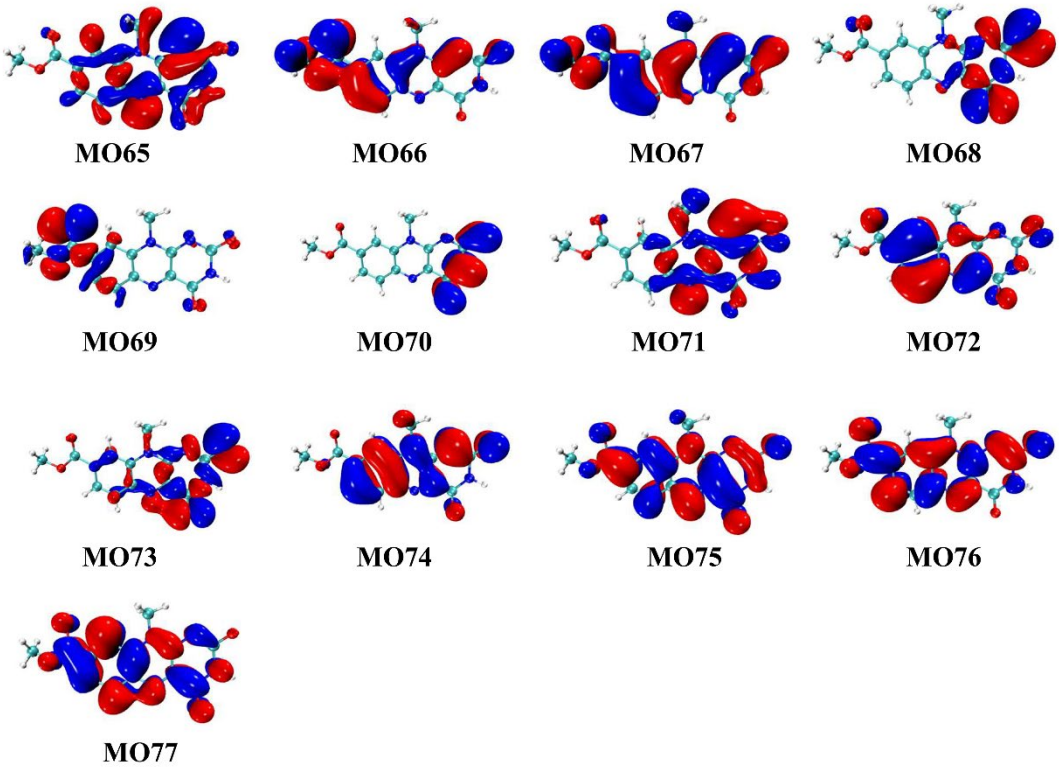

Fig. S3. Isosurface plots of frontier molecular orbitals of 8McFL involved in electron transitions contribute to UV-vis absorption. (Isovalue: ±0.02 a.u.; C: Cyan; O: Red; N: Blue; H: White.)

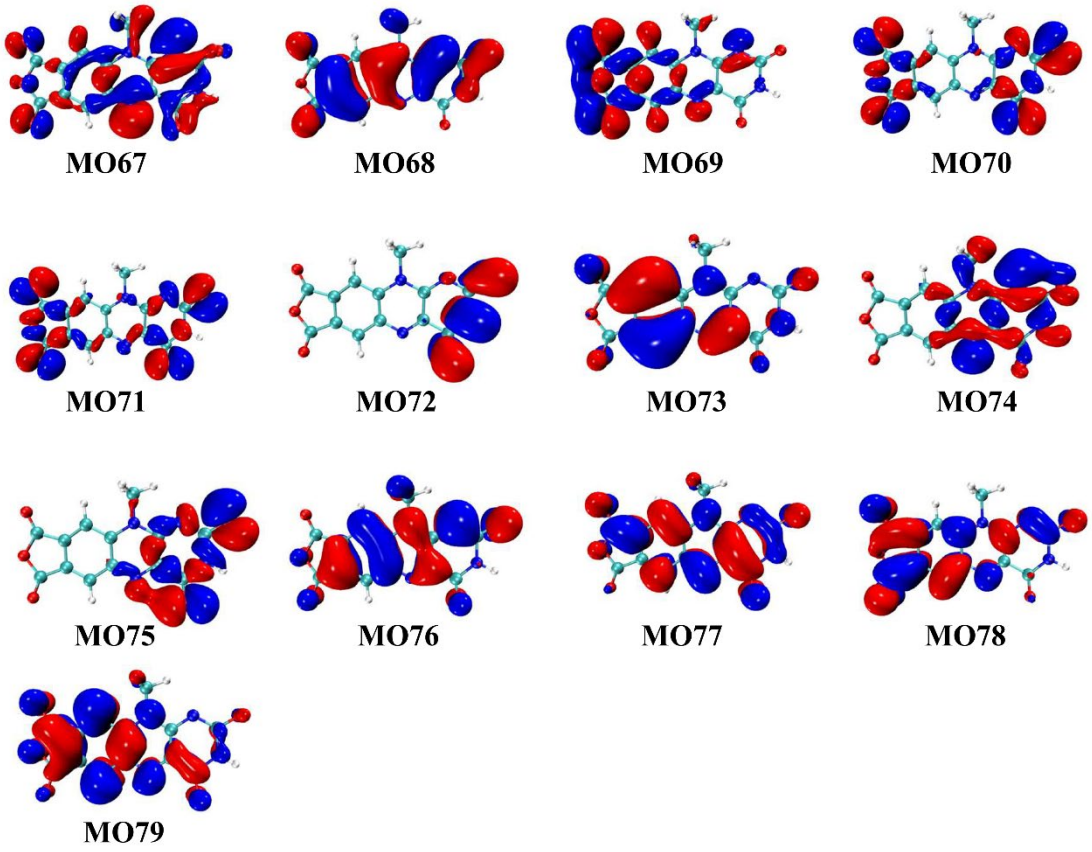

Fig. S4. Isosurface plots of frontier molecular orbitals of DcFL involved in electronic transitions contribute to UV-vis absorption. (Isovalue: ±0.02 a.u.; C: Cyan; O: Red; N: Blue; H: White.)

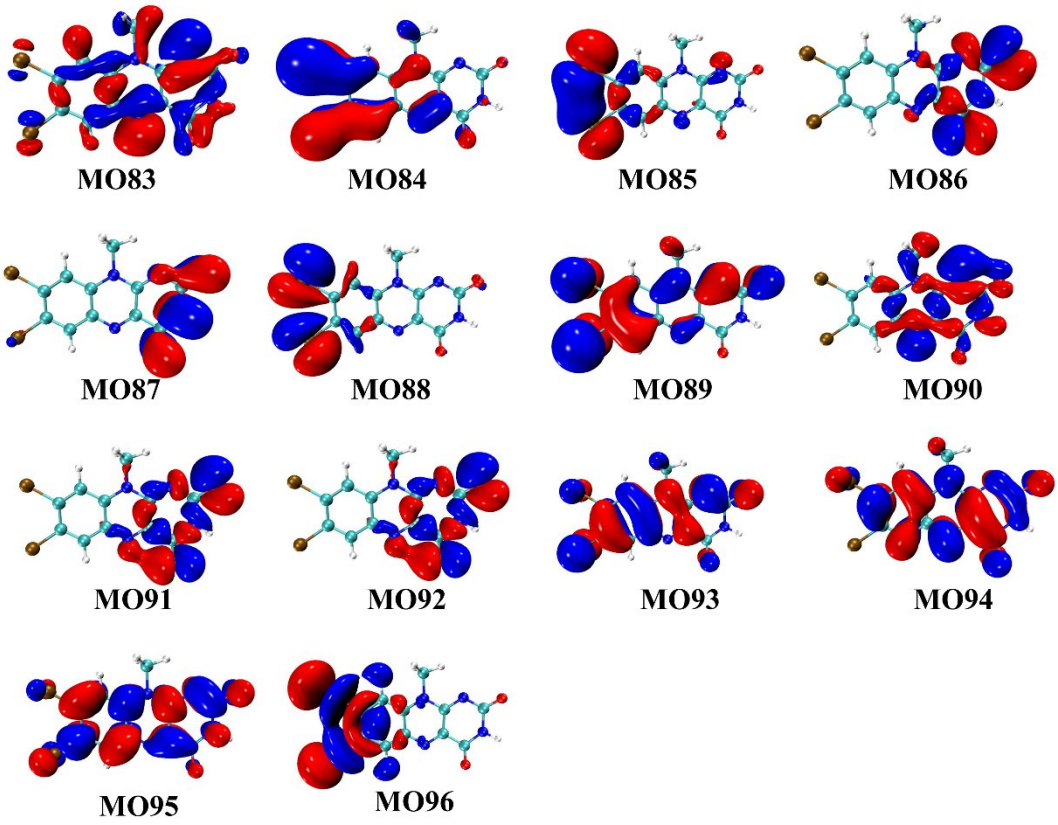

Fig. S5. Isosurface plots of frontier molecular orbitals of DBFL involved in electron transitions contribute to UV-vis absorption. (Isovalue: ±0.02 a.u.; C: Cyan; O: Red; N: Blue; H: White.)

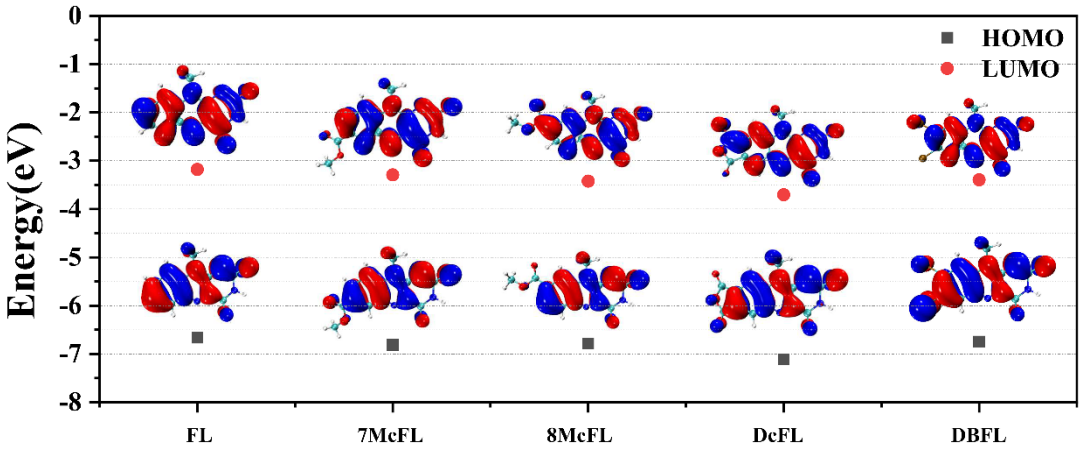

Fig. S6 Isosurface plots (Isovalue:±0.02 a.u.) and energy profile of HOMO and LUMO of McFLs

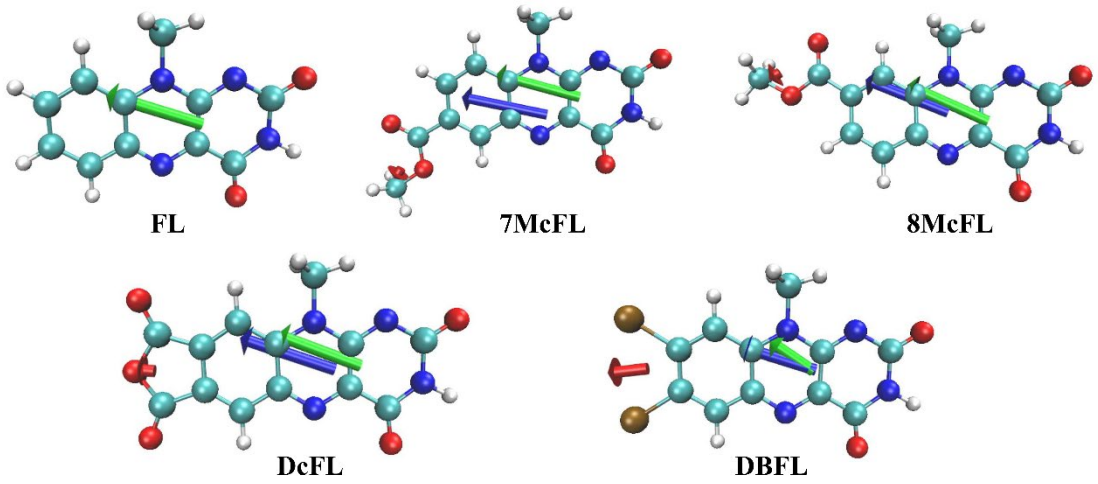

Fig. S7 Contribution of carboxy containing moiety and -Br (red), and isoalloxazine backbone (green) to μ(S_0→S_1) of McFLs (blue).

Table S6. Contribution of -COO, -Br moieties and isoalloxazine backbone to $\mu(S_0 \rightarrow S_1)$ of McFLs.

Mol	$\lvert\mu(S_0 \rightarrow S_1)\rvert$[a] (a.u.)	Contribution of isoalloxazine to $\lvert\mu(S_0 \rightarrow S_1)\rvert$ (a.u.)	Contribution of -$COOCH_3$ and -Br to $\lvert\mu(S_0 \rightarrow S_1)\rvert$ (a.u.)
FL	2.06	——	——
7McFL	2.23	2.15	0.36
8McFL	2.18	2.01	0.29
DcFL	2.08	1.57	0.57
DBFL	2.39	1.48	1.05

[a] The transition dipole moments were calculated as vectors, they were projected to calculate the contribution of -$COOCH_3$, -Br and isoalloxazine backbone. For clearance, only $|\mu|$ were presented.

Table S7. Hole-electron analysis of excited states of FL derivatives performed at B3LYP/6-311g(d) level of theory with Multiwfn.

	D/Å [a]	S_r/a.u. [b]	H/Å [c]	t/Å [d]	HDI [e]	EDI [f]
FL : S_1	1.19	0.66	2.74	-0.71	9.86	9.57
FL : T_1	0.85	0.73	2.70	-1.14	9.25	9.63
FL : T_2	0.83	1.00	2.49	-0.57	8.48	8.61
FL : T_3	0.31	0.55	2.20	-1.04	17.54	10.57
7McFL : S_1	1.18	0.66	2.82	-0.74	9.97	9.40
7McFL : T_1	0.92	0.74	2.72	-0.94	9.50	9.68
7McFL : T_2	1.23	0.83	2.53	-0.47	8.45	8.49
7McFL : T_3	0.29	0.54	2.22	-1.09	17.37	10.54
8McFL : S_1	1.31	0.66	2.90	-0.51	10.23	8.59
8McFL : T_1	1.00	0.74	2.81	-0.79	9.36	8.90
8McFL : T_2	0.84	0.95	2.61	-0.88	8.38	7.92
8McFL : T_3	0.47	0.52	2.31	-1.01	17.10	10.05
DcFL : S_1	1.70	0.64	2.95	-0.52	10.86	8.02
DcFL : T_1	1.21	0.75	2.85	-0.94	9.51	8.56
DcFL : T_2	0.52	0.53	2.35	-1.05	16.47	9.71
DcFL : T_3	0.94	0.85	2.66	-0.86	8.32	7.61
DBFL : S_1	0.67	0.81	3.03	-0.90	8.79	9.22
DBFL : T_1	0.67	0.73	2.90	-1.49	8.90	9.25
DBFL : T_2	1.25	0.83	2.65	-0.55	8.15	8.29
DBFL : T_3	0.40	0.53	2.28	-1.05	17.08	10.31

[a] The distance between centroids of hole and electron. [b] The overlap between hole and electron, calculated as $\int \sqrt{\rho^{hole}(r)\rho^{ele}(r)}\, dr$, where $\rho^{hole}(\mathbf{r})$ and $\rho^{ele}(\mathbf{r})$ are the density distribution of hole and electron, respectively. [c] Averaged root mean square derivation of spatial extension of hole and electron distribution, calculated as $H = (|\sigma_{ele}| + |\sigma_{hole}|)/2$, where $|\sigma_{ele}|$ and $|\sigma_{hole}|$ measure the overall root mean square derivation of electron and hole, respectively. [d] The degree of separation of hole and electron in the direction of charge transfer, calculated as $t = D - H_{CT}$, where D is the distance between centroids of hole and electron, and H_{CT} is the averaged degree of spatial extension of hole and electron distribution in CT direction. [e] The hole delocalization index, calculated as $100 \times \sqrt{\int [\rho^{hole}(r)]^2 dr}$. [f] The electron delocalization index, calculated as $100 \times \sqrt{\int [\rho^{ele}(r)]^2 dr}$.

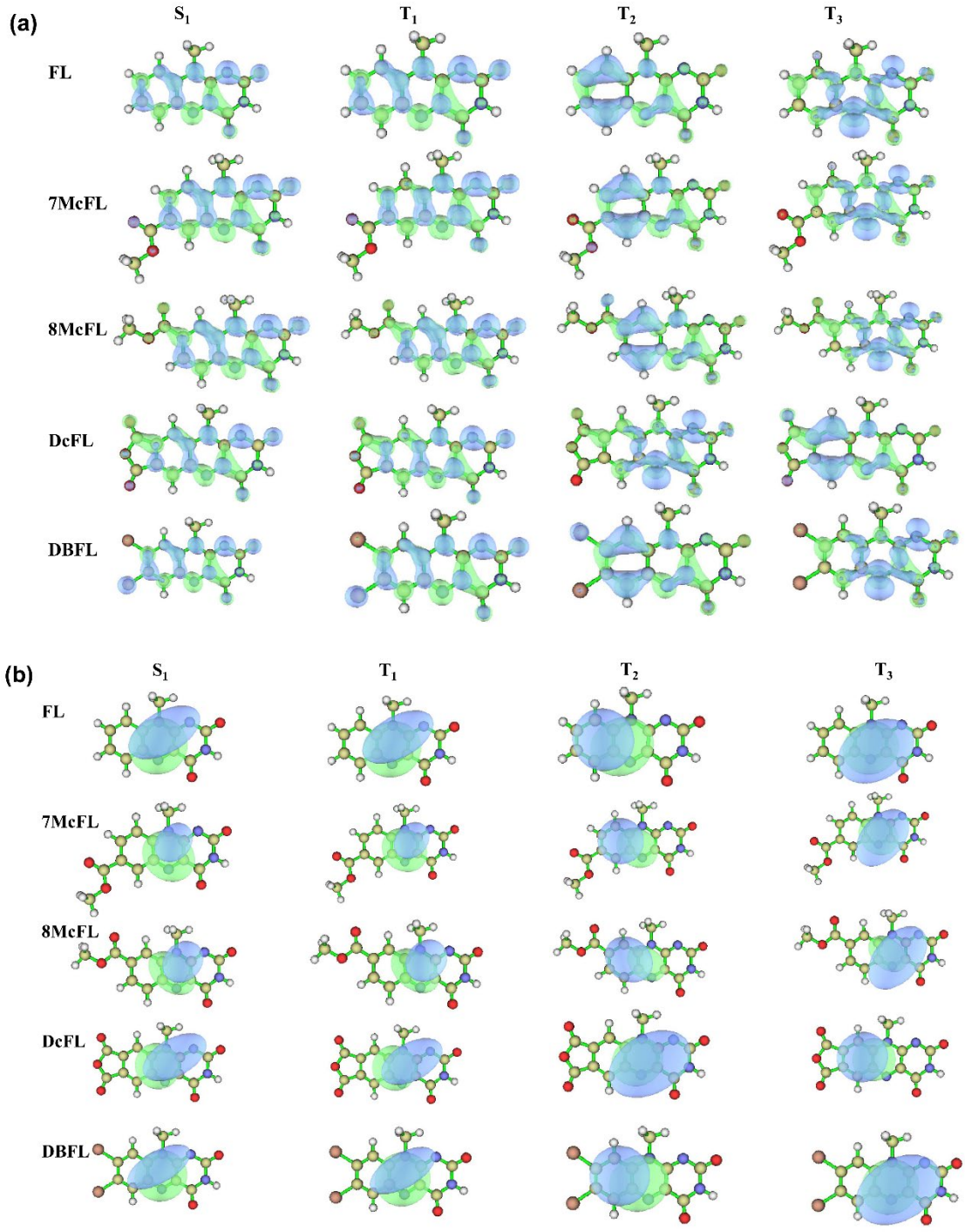

Fig. S8. Isosurface plots of hole-electron (h-e) (a) and charge density difference (CDD) (b) plots of excited states of FL, McFLs and DBFL performed at B3LYP/6-311g(d) level of theory (Isovalue: ±0.002 a.u.)

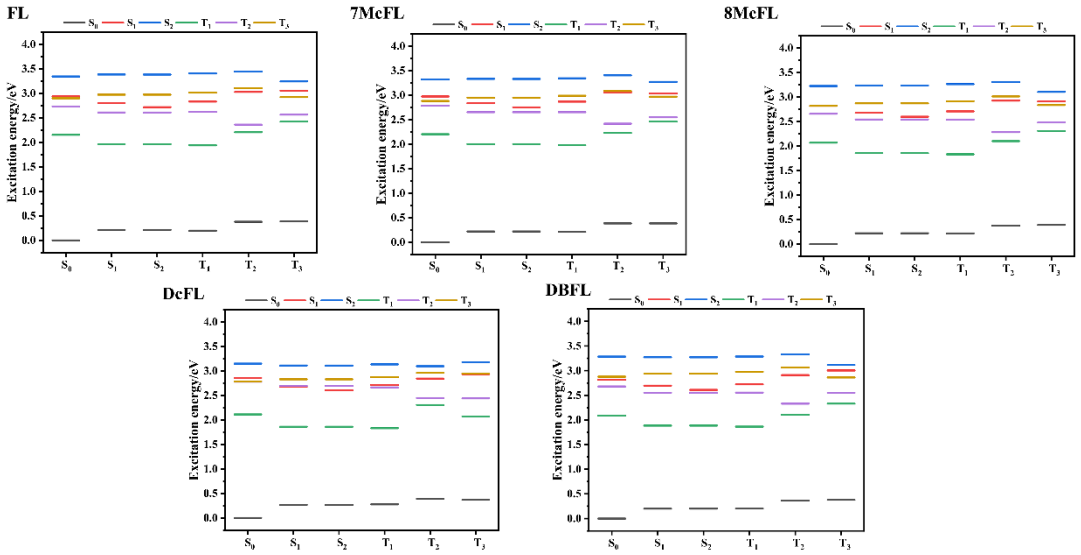

Fig. S9 Vertical excitation energy of FL derivative in CH_3CN calculated with B3LYP functional at S_0, S_1, S_2, T_1, T_2 and T_3 minimum geometry obtained at B3LYP/6-311g(d) level of theory..

Table S8. Calculated rate constants for evolution of excited McFLs in s^{-1}.

77 K	FL	7McFL	8McFL	DcFL	DBFL
$S_1 \rightarrow S_0$ k_{IC}[a]	2.26×10^{8}	3.34×10^{8}	3.42×10^{8}	1.10×10^{9}	1.70×10^{8}
$S_1 \rightarrow S_0$ k_f[b]	6.26×10^{7}	7.58×10^{7}	6.04×10^{7}	5.14×10^{7}	7.61×10^{7}
$S_1 \rightarrow T_1$ k_{ISC}[c]	1.36×10^{1}	3.92×10^{3}	5.22×10^{4}	2.73×10^{3}	2.37×10^{5}
$S_1 \rightarrow T_2$ k_{ISC}[d]	3.05×10^{6}	4.26×10^{6}	3.97×10^{6}	8.23×10^{9}	7.51×10^{5}
$S_1 \rightarrow T_3$ k'_{ISC}[e]	9.64×10^{8}	6.98×10^{9}	2.67×10^{9}	3.26×10^{6}	9.91×10^{9}
$T_1 \rightarrow S_0$ k'_{ISC}[f]	5.56×10^{3}	7.29×10^{3}	1.12×10^{4}	6.12×10^{3}	1.86×10^{0}
$T_2 \rightarrow S_0$ k'_{ISC}[g]	2.15×10^{3}	1.16×10^{3}	3.29×10^{3}	2.12×10^{2}	1.76×10^{0}
$T_3 \rightarrow S_0$ k'_{ISC}[h]	6.17×10^{4}	3.60×10^{2}	1.68×10^{3}	2.64×10^{3}	4.93×10^{4}
$T_1 \rightarrow S_0$ k_p[i]	3.25×10^{-2}	5.88×10^{-2}	2.44×10^{-2}	3.09×10^{-2}	1.77×10^{-2}
$T_2 \rightarrow S_0$ k_p[j]	6.73×10^{-2}	1.21×10^{-1}	5.73×10^{-2}	4.74×10^{-1}	1.69×10^{-2}
$T_3 \rightarrow S_0$ k_p[k]	7.97×10^{-2}	5.84×10^{-1}	2.66×10^{-1}	1.03×10^{-1}	1.84×10^{-1}
$T_2 \rightarrow T_1$ k_{IC}[l]	5.04×10^{12}	6.28×10^{12}	6.48×10^{12}	2.45×10^{12}	5.49×10^{12}
$T_3 \rightarrow T_1$ k_{IC}[m]	1.82×10^{12}	2.25×10^{12}	2.04×10^{12}	4.70×10^{12}	1.76×10^{12}
$T_3 \rightarrow T_2$ k_{IC}[n]	2.32×10^{12}	4.04×10^{11}	5.18×10^{11}	2.99×10^{9}	4.17×10^{11}

[a] Nonradiative decay rate constants for the $S_1 \rightarrow S_0$ transition; [b] Radiative decay rate constants for the $S_1 \rightarrow S_0$ transition; [c] Intersystem crossing rate constants for the $S_1 \rightarrow T_1$ transition; [d] Intersystem crossing rate constants for the $S_1 \rightarrow T_2$ transition; [e] Intersystem crossing rate constants for the $S_1 \rightarrow T_3$ transition; [f] Nonradiative decay rate constants for the $T_1 \rightarrow S_0$ transition; [g] Nonradiative decay rate constants for the $T_2 \rightarrow S_0$ transition; [h] Nonradiative decay rate constants for the $T_3 \rightarrow S_0$ transition; [i] Radiative decay rate constants for the $T_1 \rightarrow S_0$ transition; [j] Radiative decay rate constants for the $T_2 \rightarrow S_0$ transition; [k] Radiative decay rate constants for the $T_3 \rightarrow S_0$ transition; [l] Nonradiative decay rate constants for the $T_2 \rightarrow T_1$ transition; [m] Nonradiative decay rate constants for the $T_3 \rightarrow T_1$ transition; [n] Nonradiative decay rate constants for the $T_3 \rightarrow T_2$ transition;

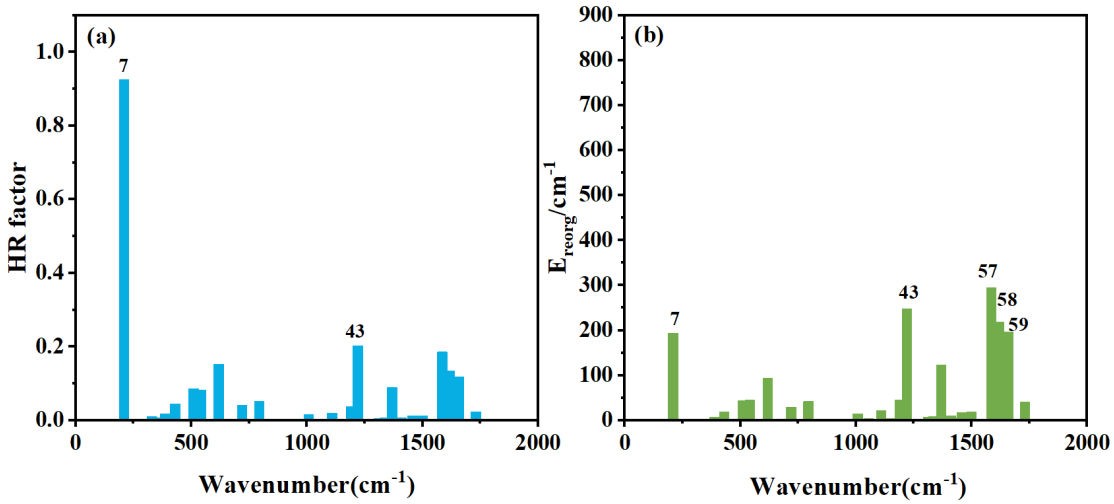

Fig. S10. Projection of HR (a) and E_{reorg} (b) of $S_1 \rightarrow S_0$ transition to S_0 vibrational normal modes of FL.

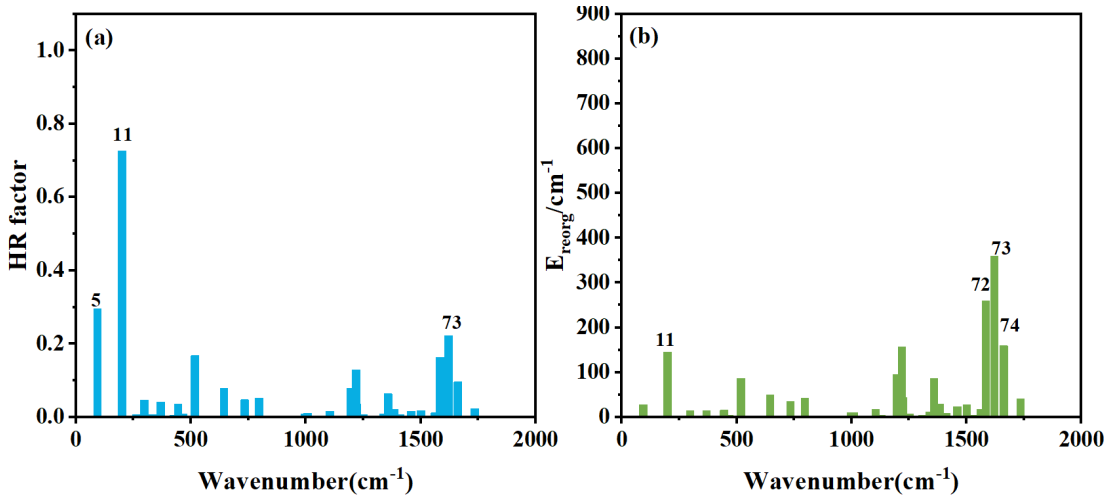

Fig. S11. Projection of HR (a) and E_{reorg} (b) of $S_1 \rightarrow S_0$ transition to S_0 vibrational normal modes of 7McFL

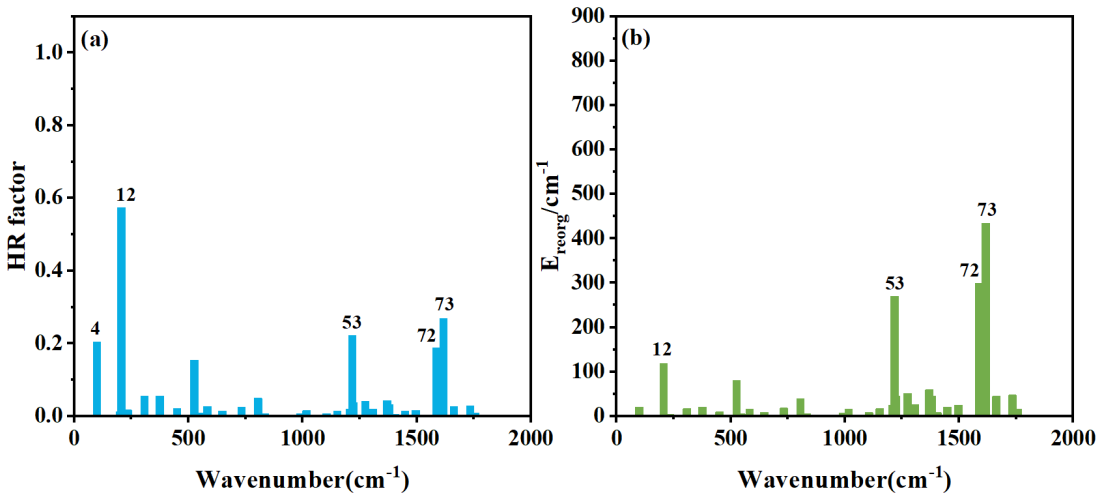

Fig. S12. Projection of HR (a) and E_{reorg} (b) of $S_1 \rightarrow S_0$ transition to S_0 vibrational normal modes of 8McFL

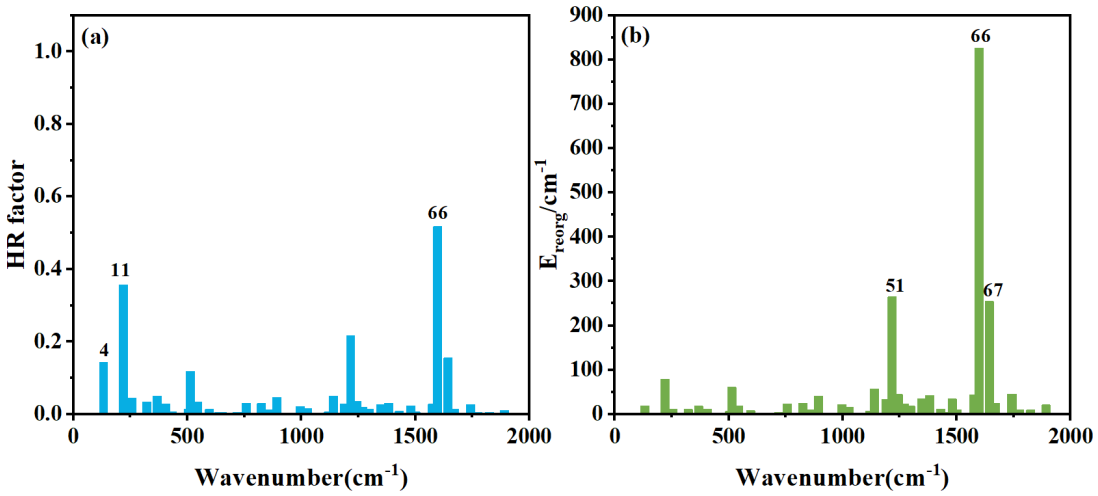

Fig. S13. Projection of HR (a) and E_{reorg} (b) of $S_1 \rightarrow S_0$ transition to S_0 vibrational normal modes of DcFL

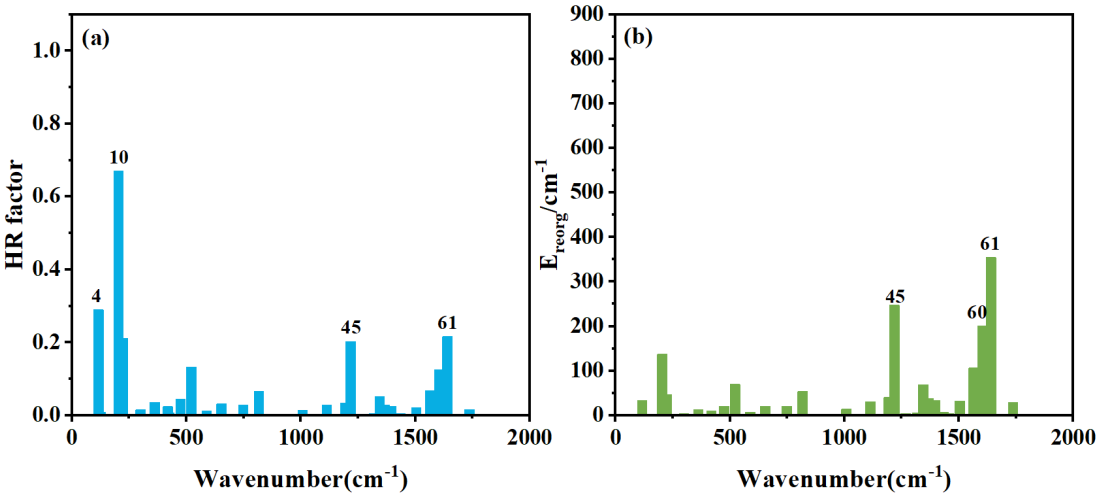

Fig. S14. Projection of HR (a) and E_{reorg} (b) of $S_1 \rightarrow S_0$ transition to S_0 vibrational normal modes of DBFL

Table S9. Projection of HR and E_{reorg} of $S_1 \rightarrow S_0$ transition to S_0 vibrational normal modes of FL.

S_0 Normal Mode	Frequency /cm^{-1}	HR factor	HR %	E_{reorg} / cm^{-1}	E_{reorg} %
7	209.08	0.93	40.09	193.43	10.83
13	430.16	0.05	2.16	19.42	1.09
15	510.76	0.08	3.45	43.60	2.44
17	540.82	0.08	3.45	44.76	2.51
20	618.67	0.15	6.47	94.17	5.27
23	719.32	0.04	1.72	29.26	1.64
28	794.58	0.05	2.16	41.71	2.34
41	1190.41	0.04	1.72	45.15	2.53
43	1220.89	0.20	8.60	247.88	13.88
47	1368.50	0.09	3.88	122.95	6.88
53	1499.71	0.01	0.43	18.69	1.05
57	1585.23	0.19	8.19	294.43	16.49
58	1618.34	0.13	5.60	218.43	12.23
59	1657.81	0.12	5.17	196.60	11.01
60	1731.35	0.02	0.86	40.88	2.29

Note: Total E_{reorg} is 1786 cm^{-1} and total HR is 2.32.

Table S10. Projection of HR and E_{reorg} of $S_1 \rightarrow S_0$ transition to S_0 vibrational normal modes of 7McFL.

S_0 Normal Mode	Frequency /cm^{-1}	HR factor	HR %	E_{reorg} / cm^{-1}	E_{reorg} %
5	93.77	0.30	12.05	27.67	1.50
11	199.90	0.73	29.32	145.21	7.89
24	518.15	0.17	6.83	86.90	4.72
28	644.79	0.08	3.21	49.97	2.72
32	733.98	0.05	2.01	34.48	1.87
36	796.35	0.05	2.01	41.65	2.26
52	1196.55	0.08	3.21	94.66	5.14
53	1218.64	0.13	5.22	156.75	8.52
54	1222.37	0.04	1.61	44.25	2.40
59	1358.15	0.06	2.41	86.02	4.68
67	1501.79	0.02	0.80	27.23	1.48
70	1529.32	0.01	0.40	4.59	0.25
71	1560.95	0.01	0.40	17.73	0.96
73	1620.76	0.22	8.84	359.77	19.55
74	1662.04	0.10	4.02	159.02	8.64

Note: Total E_{reorg} is 1840 cm^{-1} and total HR is 2.49.

Table S11. Projection of HR and E_{reorg} of $S_1 \rightarrow S_0$ transition to S_0 vibrational normal modes of 8McFL.

S_0 Normal Mode	Frequency /cm^{-1}	HR factor	HR %	E_{reorg} / cm^{-1}	E_{reorg} %
4	99.17	0.20	8.81	20.23	1.09
12	206.00	0.57	25.11	118.38	6.40
18	375.49	0.06	2.64	20.86	1.13
24	525.26	0.15	6.61	81.06	4.38
36	804.82	0.05	2.20	39.56	2.14
45	1016.97	0.02	0.88	15.69	0.85
53	1217.97	0.22	9.69	269.96	14.60
54	1223.39	0.04	1.76	45.77	2.48
55	1275.05	0.04	1.76	51.01	2.76
59	1369.37	0.04	1.76	59.27	3.21
60	1380.60	0.03	1.32	45.07	2.44
72	1587.23	0.19	8.37	298.70	16.15
73	1617.43	0.27	11.89	434.22	23.48
74	1662.78	0.03	1.32	44.93	2.43
75	1734.44	0.03	1.32	47.47	2.57

Note: Total E_{reorg} is 1849 cm^{-1} and total HR is 2.27.

Table S12. Projection of HR and E_{reorg} of $S_1 \rightarrow S_0$ transition to S_0 vibrational normal modes of DcFL.

S_0 Normal Mode	Frequency /cm^{-1}	HR factor	HR %	E_{reorg} / cm^{-1}	E_{reorg} %
4	132.56	0.14	6.22	19.05	0.86
11	220.22	0.36	16.00	78.52	3.53
12	255.65	0.04	1.78	11.42	0.51
16	367.89	0.05	2.22	18.41	0.83
21	513.66	0.12	5.33	61.02	2.74
23	543.84	0.03	1.33	18.55	0.83
33	757.87	0.03	1.33	23.06	1.04
41	892.56	0.05	2.22	40.86	1.84
48	1139.55	0.05	2.22	57.51	2.58
50	1189.87	0.03	1.33	33.58	1.51
51	1216.44	0.22	9.78	264.69	11.89
52	1243.24	0.04	1.78	44.84	2.01
66	1597.64	0.52	23.11	826.07	37.11
67	1642.79	0.16	7.11	254.86	11.45
69	1742.33	0.03	1.33	45.55	2.05

Note: Total E_{reorg} is 2226 cm^{-1} and total HR is 2.25.

Table S13. Projection of HR and E_{reorg} of $S_1 \rightarrow S_0$ transition to S_0 vibrational normal modes of DBFL.

S_0 Normal Mode	Frequency /cm^{-1}	HR factor	HR %	E_{reorg} / cm^{-1}	E_{reorg} %
4	115.99	0.29	11.93	33.64	2.01
10	204.22	0.67	27.57	137.01	8.19
11	223.55	0.21	8.64	47.13	2.82
20	474.27	0.04	1.65	20.70	1.24
22	522.37	0.13	5.35	69.58	4.16
26	653.79	0.03	1.23	20.57	1.23
30	747.81	0.03	1.23	20.80	1.24
41	1113.9	0.03	1.23	31.04	1.86
44	1194.17	0.03	1.23	40.72	2.43
45	1217.8	0.20	8.23	247.00	14.76
49	1344.61	0.05	2.06	68.71	4.11
50	1366.52	0.03	1.23	37.92	2.27
59	1564.84	0.07	2.88	106.14	6.34
60	1604.42	0.13	5.35	201.36	12.04
61	1640.31	0.22	9.05	354.26	21.18

Note: Total E_{reorg} is 1673 cm^{-1} and total HR is 2.43.

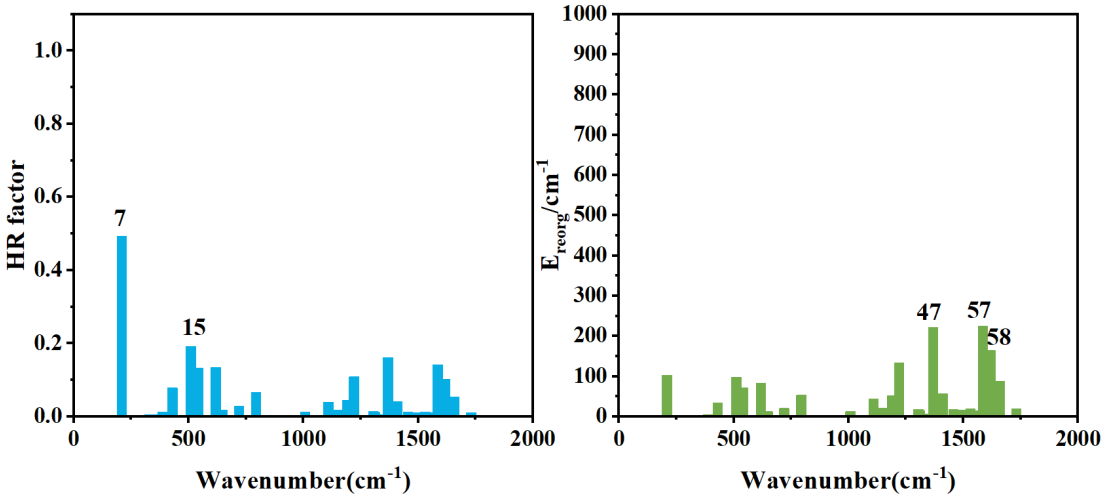

Fig. S15. Projection of HR (a) and E_{reorg} (b) of $T_1 \rightarrow S_0$ transition to S_0 vibrational normal modes of FL.

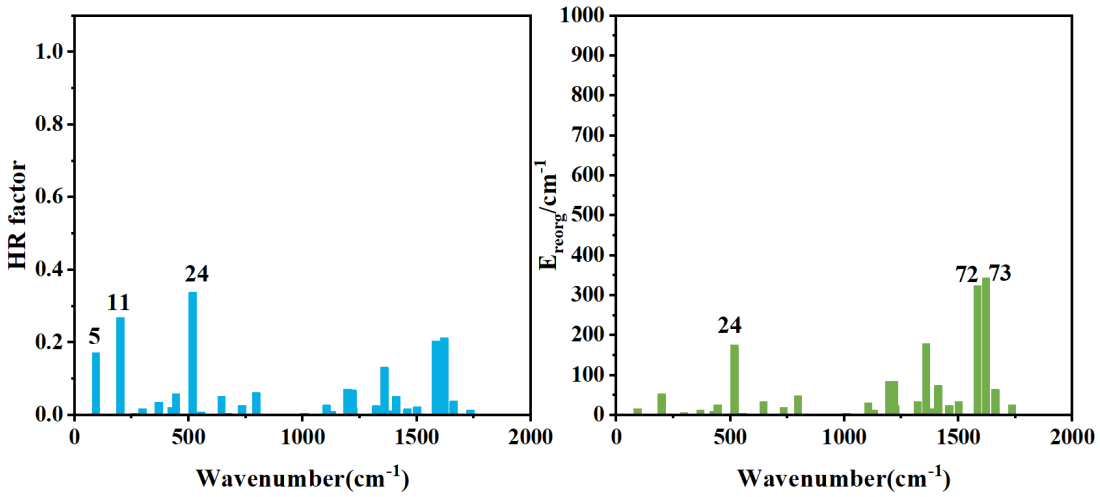

Fig. S16. Projection of HR (a) and E_{reorg} (b) of $T_1 \rightarrow S_0$ transition to S_0 vibrational normal modes of 7McFL.

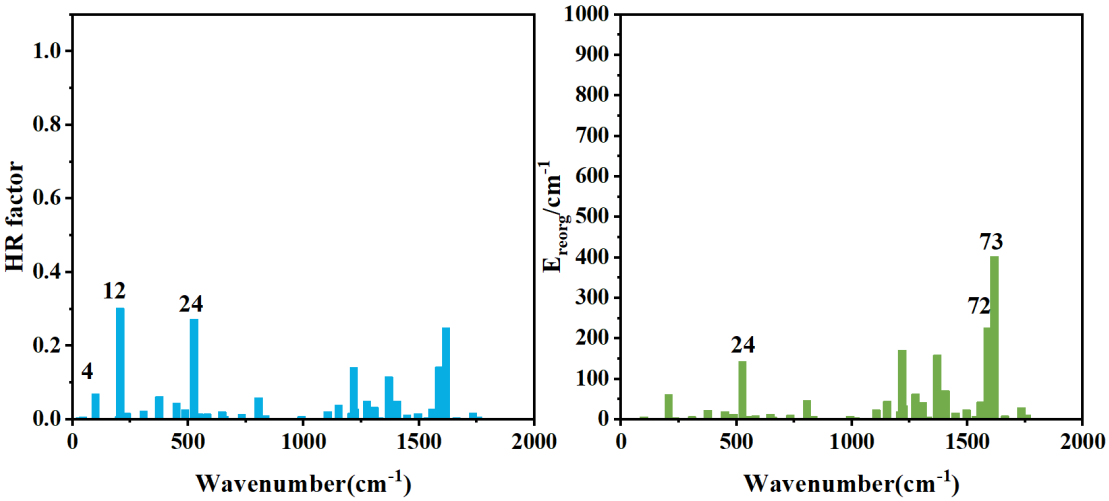

Fig. S17. Projection of HR (a) and E_{reorg} (b) of $T_1 \rightarrow S_0$ transition to S_0 vibrational normal modes of 8McFL.

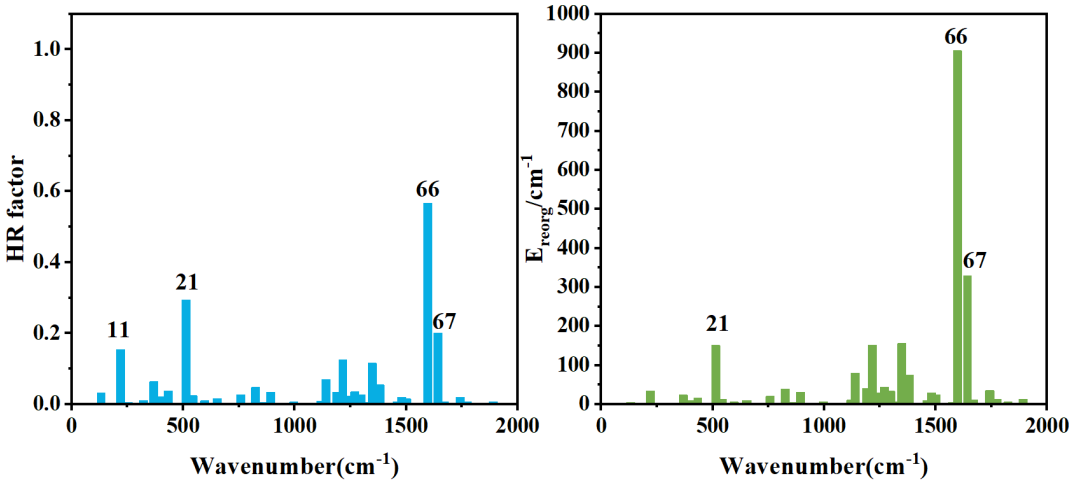

Fig. S18. Projection of HR (a) and E_{reorg} (b) of $T_1 \rightarrow S_0$ transition to S_0 vibrational normal modes of DcFL.

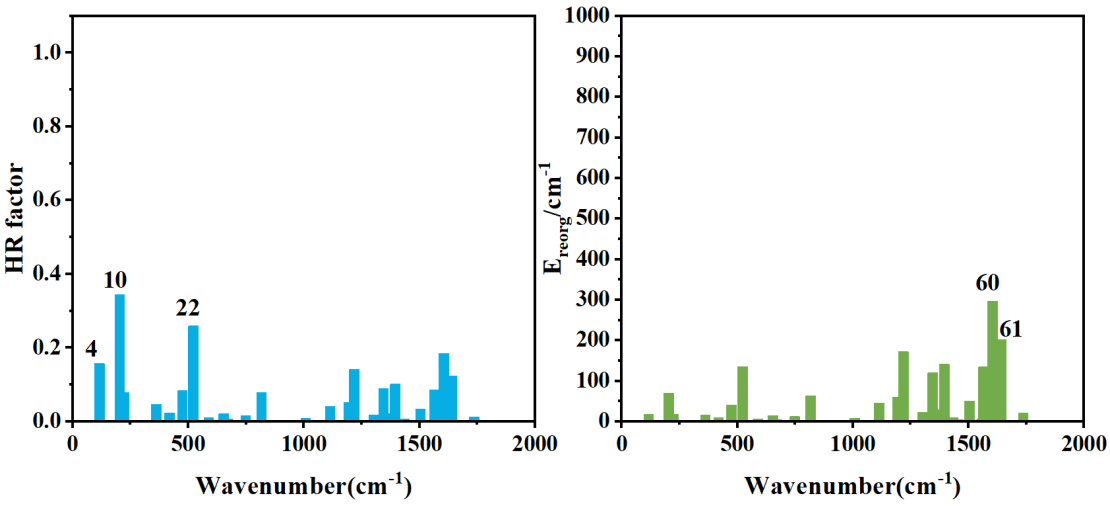

Fig. S19. Projection of HR (a) and E_{reorg} (b) of $T_1 \rightarrow S_0$ transition to S_0 vibrational normal modes of DBFL.

Table S14. Projection of HR and E_{reorg} of $T_1 \rightarrow S_0$ transition to S_0 vibrational normal modes of FL.

S_0 Normal Mode	Frequency /cm^{-1}	HR factor	HR %	E_{reorg} / cm^{-1}	E_{reorg} %
7	209.08	0.49	24.38	102.99	6.13
13	430.16	0.08	3.98	33.68	2.00
15	510.76	0.19	9.45	97.91	5.83
17	540.82	0.13	6.47	71.60	4.26
20	618.67	0.14	6.97	83.33	4.96
23	719.32	0.03	1.49	20.18	1.20
28	794.58	0.07	3.48	52.86	3.15
38	1108.81	0.04	1.99	44.03	2.62
41	1190.41	0.04	1.99	52.34	3.12
43	1220.89	0.11	5.47	132.80	7.90
47	1368.50	0.16	7.96	220.91	13.15
49	1410.43	0.04	1.99	56.47	3.36
57	1585.23	0.14	6.97	224.91	13.39
58	1618.34	0.10	4.98	164.24	9.78
59	618.67	0.14	6.97	83.33	4.96

Note: Total E_{reorg} is 1680 cm^{-1} and total HR is 2.01.

Table S15. Projection of HR and E_{reorg} of $T_1 \rightarrow S_0$ transition to S_0 vibrational normal modes of 7McFL.

S_0 Normal Mode	Frequency /cm^{-1}	HR factor	HR %	E_{reorg} / cm^{-1}	E_{reorg} %
5	93.77	0.17	8.25	16.08	0.89
11	199.90	0.27	13.11	53.80	2.97
18	369.16	0.04	1.94	13.20	0.73
21	444.22	0.06	2.91	26.15	1.44
24	518.15	0.34	16.50	175.29	9.69
28	644.79	0.05	2.43	33.44	1.85
36	796.35	0.06	2.91	49.32	2.73
52	1196.55	0.07	3.40	85.02	4.70
53	1218.64	0.07	3.40	84.18	4.65
59	1358.15	0.13	6.31	179.00	9.89
61	1411.31	0.05	2.43	73.75	4.08
67	1501.79	0.02	0.97	33.88	1.87
72	1584.16	0.20	9.71	323.22	17.87
73	1620.76	0.21	10.19	343.96	19.01
74	1662.04	0.04	1.94	64.77	3.58

Note: Total E_{reorg} is 1809 cm^{-1} and total HR is 2.06.

Table S16. Projection of HR and E_{reorg} of $T_1 \rightarrow S_0$ transition to S_0 vibrational normal modes of 8McFL.

S_0 Normal Mode	Frequency /cm^{-1}	HR factor	HR %	E_{reorg} / cm^{-1}	E_{reorg} %
4	99.17	0.07	3.45	6.82	0.36
12	206.00	0.30	14.78	62.29	3.32
18	375.49	0.06	2.96	23.17	1.24
21	450.82	0.04	1.97	20.00	1.07
24	525.26	0.27	13.30	142.97	7.63
36	804.82	0.06	2.96	47.35	2.53
49	1152.53	0.04	1.97	45.00	2.40
53	1217.97	0.14	6.90	171.07	9.12
54	1223.39	0.03	1.48	33.75	1.80
59	1369.37	0.12	5.91	158.68	8.46
60	1380.60	0.03	1.48	35.40	1.89
61	1405.05	0.05	2.46	71.20	3.80
71	1557.53	0.03	1.48	43.21	2.30
72	1587.23	0.14	6.90	226.00	12.05
73	1617.43	0.25	12.32	402.35	21.46

Note: Total E_{reorg} is 1875 cm^{-1} and total HR is 2.03.

Table S17. Projection of HR and E_{reorg} of $T_1 \rightarrow S_0$ transition to S_0 vibrational normal modes of DcFL.

S_0 Normal Mode	Frequency /cm^{-1}	HR factor	HR %	E_{reorg} / cm^{-1}	E_{reorg} %
4	132.56	0.03	1.40	4.25	0.18
11	220.22	0.15	6.98	33.90	1.42
16	367.89	0.06	2.79	23.27	0.97
21	513.66	0.29	13.49	150.90	6.31
38	824.96	0.05	2.33	39.23	1.64
41	892.56	0.03	1.40	30.59	1.28
48	1139.55	0.07	3.26	80.05	3.35
50	1189.87	0.03	1.40	40.90	1.71
51	1216.44	0.13	6.05	152.17	6.36
52	1243.24	0.02	0.93	29.18	1.22
53	1269.80	0.04	1.86	44.55	1.86
56	1348.25	0.12	5.58	155.69	6.51
57	1381.92	0.05	2.33	75.41	3.15
66	1597.64	0.57	26.51	905.68	37.88
67	1642.79	0.20	9.30	329.42	13.78

Note: Total E_{reorg} is 2391 cm^{-1} and total HR is 2.15.

Table S18. Projection of HR and E_{reorg} of $T_1 \rightarrow S_0$ transition to S_0 vibrational normal modes of DBFL.

S_0 Normal Mode	Frequency /cm^{-1}	HR factor	HR %	E_{reorg} / cm^{-1}	E_{reorg} %
4	115.99	0.16	7.77	18.22	1.05
10	204.22	0.34	16.50	70.41	4.04
15	361.60	0.05	2.43	16.74	0.96
20	474.27	0.08	3.88	39.90	2.29
22	522.37	0.26	12.62	135.39	7.77
33	817.19	0.08	3.88	63.40	3.64
41	1113.90	0.04	1.94	46.22	2.65
44	1194.17	0.05	2.43	60.79	3.49
45	1217.80	0.14	6.80	172.05	9.88
49	1344.61	0.09	4.37	119.69	6.87
51	1395.11	0.10	4.85	141.25	8.11
56	1504.30	0.03	1.46	50.02	2.87
59	1564.84	0.09	4.37	135.05	7.75
60	1604.42	0.19	9.22	297.03	17.05
61	1640.31	0.12	5.83	202.38	11.62

Note: Total E_{reorg} is 1742 cm^{-1} and total HR is 2.06.

Table S19. Calculated rates for evolution of excited McFLs in mol·L^{-1}·s^{-1}.

298 K	FL	7McFL	8McFL	DcFL	DBFL
$S_1 \rightarrow S_0$ R_{IC}[a]	2.24	1.56	5.97×10^{-1}	3.56×10^{1}	1.50×10^{-2}
$S_1 \rightarrow S_0$ R_f[b]	5.82×10^{-1}	2.21×10^{-1}	9.09×10^{-2}	2.79×10^{-1}	1.03×10^{-2}
$S_1 \rightarrow T_1$ R_{ISC}[c]	2.76×10^{-7}	2.08×10^{-7}	1.79×10^{-7}	1.72×10^{-8}	3.84×10^{-7}
$S_1 \rightarrow T_2$ R_{ISC}[d]	4.23×10^{-2}	1.22×10^{-2}	6.72×10^{-3}	4.09×10^{1}	9.16×10^{-5}
$S_1 \rightarrow T_3$ R_{ISC}[e]	8.18	1.49×10^{1}	3.12	2.91×10^{-2}	2.21
$T_1 \rightarrow S_0$ R'_{ISC}[f]	7.75	1.47×10^{1}	3.12×10^{1}	4.10×10^{2}	1.27×10^{-2}
$T_2 \rightarrow S_0$ R'_{ISC}[g]	2.46×10^{-9}	1.51×10^{-9}	5.29×10^{-9}	4.43×10^{-8}	1.30×10^{-13}
$T_3 \rightarrow S_0$ R'_{ISC}[h]	1.81×10^{-5}	2.24×10^{-7}	1.74×10^{-6}	6.24×10^{-12}	2.49×10^{-13}
$T_1 \rightarrow S_0$ R_p[i]	8.35×10^{-4}	1.52×10^{-3}	4.99×10^{-4}	1.88×10^{-2}	5.49×10^{-4}
$T_2 \rightarrow S_0$ R_p[j]	2.20×10^{-14}	4.26×10^{-14}	4.94×10^{-14}	4.30×10^{-12}	8.52×10^{-16}
$T_3 \rightarrow S_0$ R_p[k]	4.58×10^{-12}	2.12×10^{-12}	2.21×10^{-12}	7.14×10^{-16}	2.49×10^{-13}
$T_2 \rightarrow T_1$ R_{IC}[l]	2.19	2.13	6.32	4.09×10^{1}	3.36×10^{-1}
$T_3 \rightarrow T_1$ R_{IC}[m]	6.03	1.27×10^{1}	2.50×10^{1}	2.26×10^{-2}	1.26
$T_3 \rightarrow T_2$ R_{IC}[n]	2.15	2.12	6.25	4.74×10^{-3}	3.36×10^{-1}
$T_1 \rightarrow S_1$ R_{RISC} [o]	4.57×10^{-1}	8.17×10^{-2}	4.00×10^{-1}	9.34×10^{-2}	1.58
$T_2 \rightarrow S_1$ R_{RISC} [p]	3.41×10^{-10}	7.10×10^{-12}	2.63×10^{-11}	9.29×10^{-6}	7.34×10^{-13}
$T_3 \rightarrow S_1$ R_{RISC} [q]	1.09×10^{-4}	4.14×10^{-6}	2.54×10^{-4}	9.04×10^{-11}	1.02×10^{-3}

[a] $S_1 \rightarrow S_0$ IC rate; [b] $S_1 \rightarrow S_0$ FE rate; [c] $S_1 \rightarrow T_1$ ISC rate; [d] $S_1 \rightarrow T_2$ ISC rate; [e] $S_1 \rightarrow T_3$ ISC rate; [f] Nonradiative decay rate for the $T_1 \rightarrow S_0$ transition; [g] Nonradiative decay rate for the $T_2 \rightarrow S_0$ transition; [h] Nonradiative decay rate for the $T_3 \rightarrow S_0$ transition; [i] $T_1 \rightarrow S_0$ PE rate; [j] $T_2 \rightarrow S_0$ PE rate; [k] $T_3 \rightarrow S_0$ PE rate; [l] $T_2 \rightarrow T_1$ IC rate; [m] $T_3 \rightarrow T_1$ IC rate; [n] $T_3 \rightarrow T_2$ IC rate; [o] $T_1 \rightarrow S_1$ reverse ISC rate; [p] $T_2 \rightarrow S_1$ reverse ISC rate; [q] $T_3 \rightarrow S_1$ reverse ISC rate.

REFERENCES:

1. R. C. Binning and L. A. Curtiss, *J. Comput. Chem.*, 1990, **11**, 1206-1216.
2. M. M. Francl, W. J. Pietro, W. J. Hehre, J. S. Binkley, M. S. Gordon, D. J. Defrees and J. A. Pople, *J. Chem. Phys.*, 1982, **77**, 3654-3665.
3. A. D. Becke, *J. Chem. Phys.*, 1993, **98**, 5648-5652.
4. C. T. Lee, W. T. Yang and R. G. Parr, *Phys. Rev. B*, 1988, **37**, 785-789.
5. S. Miertus, E. Scrocco and J. Tomasi, *Chem. Phys.*, 1981, **55**, 117-129.
6. R. Cammi and B. Mennucci, *J. Chem. Phys.*, 1999, **110**, 9877-9886.
7. J. Tomasi, B. Mennucci and R. Cammi, *Chem. Rev.*, 2005, **105**, 2999-3093.
8. M. J. Frisch, G. W. Trucks, H. B. Schlegel, G. E. Scuseria, M. A. Robb, J. R. Cheeseman, G. Scalmani, V. Barone, G. A. Petersson, H. Nakatsuji, X. Li, M. Caricato, A. V. Marenich, J. Bloino, B. G. Janesko, R. Gomperts, B. Mennucci, H. P. Hratchian, J. V. Ortiz, A. F. Izmaylov, J. L. Sonnenberg, Williams, F. Ding, F. Lipparini, F. Egidi, J. Goings, B. Peng, A. Petrone, T. Henderson, D. Ranasinghe, V. G. Zakrzewski, J. Gao, N. Rega, G. Zheng, W. Liang, M. Hada, M. Ehara, K. Toyota, R. Fukuda, J. Hasegawa, M. Ishida, T. Nakajima, Y. Honda, O. Kitao, H. Nakai, T. Vreven, K. Throssell, J. A. Montgomery Jr., J. E. Peralta, F. Ogliaro, M. J. Bearpark, J. J. Heyd, E. N. Brothers, K. N. Kudin, V. N. Staroverov, T. A. Keith, R. Kobayashi, J. Normand, K. Raghavachari, A. P. Rendell, J. C. Burant, S. S. Iyengar, J. Tomasi, M. Cossi, J. M. Millam, M. Klene, C. Adamo, R. Cammi, J. W. Ochterski, R. L. Martin, K. Morokuma, O. Farkas, J. B. Foresman and D. J. Fox, *Gaussian 16 A03*, 2016.
9. O. Vahtras, H. Agren, P. Jorgensen, H. J. A. Jensen, T. Helgaker and J. Olsen, *J. Chem. Phys.*, 1992, **97**, 9178-9187.
10. H. Hettema, H. J. A. Jensen, P. Jorgensen and J. Olsen, *J. Chem. Phys.*, 1992, **97**, 1174-1190.
11. H. Agren, O. Vahtras, H. Koch, P. Jorgensen and T. Helgaker, *J. Chem. Phys.*, 1993, **98**, 6417-6423.
12. J. Olsen, D. L. Yeager and P. Jorgensen, *J. Chem. Phys.*, 1989, **91**, 381-388.
13. P. Jorgensen, H. J. A. Jensen and J. Olsen, *J. Chem. Phys.*, 1988, **89**, 3654-3661.
14. K. Aidas, C. Angeli, K. L. Bak, V. Bakken, R. Bast, L. Boman, O. Christiansen, R. Cimiraglia, S. Coriani, P. Dahle, E. K. Dalskov, U. Ekstrom, T. Enevoldsen, J. J. Eriksen, P. Ettenhuber, B. Fernandez, L. Ferrighi, H. Fliegl, L. Frediani, K. Hald, A. Halkier, C. Hattig, H. Heiberg, T. Helgaker, A. C. Hennum, H. Hettema, E. Hjertenaes, S. Host, I. M. Hoyvik, M. F. Iozzi, B. Jansik, H. J. A. Jensen, D. Jonsson, P. Jorgensen, J. Kauczor, S. Kirpekar, T. Kjrgaard, W. Klopper, S. Knecht, R. Kobayashi, H. Koch, J. Kongsted, A. Krapp, K. Kristensen, A. Ligabue, O. B. Lutnaes, J. I. Melo, K. V. Mikkelsen, R. H. Myhre, C. Neiss, C. B. Nielsen, P. Norman, J. Olsen, J. M. H. Olsen, A. Osted, M. J. Packer, F. Pawlowski, T. B. Pedersen, P. F. Provasi, S. Reine, Z. Rinkevicius, T. A. Ruden, K. Ruud, V. V. Rybkin, P. Salek, C. C. M. Samson, A. S. de Meras, T. Saue, S. P. A. Sauer, B. Schimmelpfennig, K. Sneskov, A. H. Steindal, K. O. Sylvester-Hvid, P. R. Taylor, A. M. Teale, E. I. Tellgren, D. P. Tew, A. J. Thorvaldsen, L. Thogersen, O. Vahtras, M. A. Watson, D. J. D. Wilson, M. Ziolkowski and H. Agren, *Wiley Interdiscip. Rev.-Comput. Mol. Sci.*, 2014, **4**, 269-284.
15. Q. Peng, Y. P. Yi, Z. G. Shuai and J. S. Shao, *J. Chem. Phys.*, 2007, **126**, 114302.
16. Q. Peng, Y. P. Yi, Z. G. Shuai and J. S. Shao, *J. Am. Chem. Soc.*, 2007, **129**, 9333-9339.
17. Y. L. Niu, Q. A. Peng, C. M. Deng, X. Gao and Z. G. Shuai, *J. Phys. Chem. A*, 2010, **114**, 7817-7831.

18. Y. Niu, Q. Peng and Z. Shuai, *Sci. China Ser. B-Chem.*, 2008, **51**, 1153-1158.
19. Q. Peng, Y. L. Niu, Q. H. Shi, X. Gao and Z. G. Shuai, *J. Chem. Theory Comput.*, 2013, **9**, 1132-1143.
20. Hongzhiwei Technology, *Device Studio 2021A*, 2021, Available online: https://iresearch.net.cn/cloudSoftware (accessed on 2021-10-12).
21. Z. G. Shuai, *Chin. J. Chem.*, 2020, **38**, 1223-1232.
22. Y. L. Niu, W. Q. Li, Q. Peng, H. Geng, Y. P. Yi, L. J. Wang, G. J. Nan, D. Wang and Z. G. Shuai, *Mol. Phys.*, 2018, **116**, 1078-1090.
23. Z. G. Shuai and Q. Peng, *Phys. Rep.-Rev. Sec. Phys. Lett.*, 2014, **537**, 123-156.
24. Z. G. Shuai and Q. Peng, *Natl. Sci. Rev.*, 2017, **4**, 224-239.
25. Y. Niu, Q. Peng, C. Deng, X. Gao and Z. Shuai, *J. Phys. Chem. A*, 2010, **114**, 7817-7831.